Infrared properties of high-T_c superconductors

T. Timusk and D.B. Tanner

in

Physical Properties of High-Temperature Superconductors I,

edited by Donald M. Ginsberg

(World Scientific, Singapore, 1989)

pp. 339–407.

Infrared properties of high T_c superconductors

Thomas Timusk

Department of Physics, McMaster University, Hamilton, Ont. Canada, L8S 4M1

David B. Tanner

Department of Physics, University of Florida, Gainesville, FL 32611, USA

ABSTRACT: The infrared properties of the high T_c superconductors are reviewed. We place particular emphasis on attempts to determine the energy gap by far infrared spectroscopy and on the properties of the strong absorption that occurs in the mid infrared. We conclude that although the energy gap is not easily observed, several recent experiments place it close to the BCS weak-coupling value of $2\Delta/k_BT_c$=3.5. We show that the dramatic reflectance edge observed in many far-infrared experiments is *not* the gap; rather than the onset of absorption, it is due to strong dispersion in the real part of the dielectric function: i.e., a plasma edge. This dispersion is caused by the presence of a strong absorption in the mid-infrared region. We argue that this mid-infrared absorption is a direct particle-hole excitation rather than a Holstein emission process.

A Review for *The Physical Properties of High-Temperature Superconductors*, D.M. Ginsberg, editor, (World Scientific Publishing Company).

I. INTRODUCTION

Soon after the discovery of high temperature superconductivity by Bednorz and Müller[1] attempts were made to find the energy gap and any spectral features responsible for the superconducting pairing by infrared spectroscopy, a technique that had been used with success in the classic superconductors. In addition, several studies of the basic optical properties of these materials were made, with the goal of obtaining information about the electronic band structure, low-lying excitations, phonon frequencies, etc. There has been a large amount of subsequent work, showing that the infrared properties of these materials are extremely complicated, and at the time of the writing of this review our understanding is still incomplete. These experiments are the subject of this review.

According to the BCS theory, a bulk superconductor at low temperature is a perfect reflector of electromagnetic energy at frequencies below its superconducting energy gap. Above this frequency it behaves much like a normal metal. Ordinary superconductors live up to this expectation extremely well. Some of the earliest spectroscopic evidence for an energy gap in ordinary superconductors was obtained by infrared and microwave spectroscopy. In low gap materials such as aluminum Biondi and Garfunkel[2] employed microwave spectroscopy to find an onset of absorption at the gap frequency. Approaching the problem from the infrared side Tinkham's group with Glover[3], Ginsberg[4] and Richards[5] measured the gap in lead and tin. In each case absorption occurred only at or above the superconducting gap frequency. At substantially higher frequencies, the optical properties of a superconductor were found to be independent of the transition to the superconducting state.

A second use of far infrared spectroscopy in superconductivity came from the discovery by Joyce and Richards[6] of phonon structure in the spectrum of the strong-coupling superconductor lead. Predicted by Holstein[7] long before, this process of phonon emission produces a spectrum that is closely related to the Eliashberg function $\alpha^2 F(\Omega)$ seen in tunnelling spectroscopy.[8,9] Here $F(\Omega)$ is the phonon density of states and α is the coupling constant of the electron phonon interaction. Thus, in principle, one can find the spectrum of excitations responsible for superconductivity from a detailed study of the infrared spectrum.

An important final use of infrared and optical spectroscopy in the study of ordinary materials is the determination of electronic and vibrational properties: plasmons, interband transitions, and free-carrier absorption all give a view into the electronic band structure of a material. Lattice vibrations, electron-phonon interactions, etc., also provide fundamental information about the nature of a substance.

However, the new materials present a real challenge to the spectroscopist. They exhibit both metallic and insulating behavior. They show large optical anisotropy. The samples come in forms not ideal for precision spectroscopy: powders, porous ceramics, irregular mosaics of small twinned crystals and thin films on substrates with complicated optical properties of their own. Added to this complexity is the domain structure of $YBa_2Cu_3O_{7-\delta}$ crystals. The presence of a twin pattern in the crystal morphology of this most common high-temperature superconductor means that all measurements (even polarized optical measurements on crystals) will see a complicated effective average of the **a** and **b** dielectric functions.

In this review we survey the application of infrared techniques to the study of high temperature superconductors. Issues include the magnitude of the energy gap, the search for a Holstein spectrum of the superconducting excitations, and the nature of low- lying electronic states. At the time of writing, October 1988, none of these problems has been solved but some progress can be reported. A consensus is emerging that the energy gap is in the neighborhood of $3.5k_BT_c$, the weak coupling BCS value, and that the excitations are at very high frequency and rather weakly coupled to the electrons. The observations are consistent with a weak coupling BCS mechanism involving electronic excitations.

A further consensus exists that the simple Drude model is inadequate to describe the **ab**-plane optical response. The dc and low frequency conductivities are rather different (in terms of temperature dependence, lifetime, and oscillator strength) from the mid- and near-infrared absorption processes.

We start in section II with a review of the elementary theory of the optical constants of solids, particularly metals and superconductors. In section III we deal with the controversial midinfrared absorption, the so-called "0.5 eV" peak. First discovered in the polycrystalline samples of $La_{2-x}Sr_xCuO_4$ this absorption

seems to be a common feature of all the high temperature superconductors. We will review the various interpretations of this excess infrared absorption.

Section IV contains a review of some of the work that has been devoted to the search for the energy gap. We cannot in the available space adequately consider the large number of papers that have addressed the topic, particularly on the polycrystalline ceramics; we therefore will focus more on the recent work that is available to us on **ab**-plane oriented samples.

We conclude in section V with an assessment of the current state of the experimental situation and with some comments about work needing to be done.

II. OPTICAL PROPERTIES OF SUPERCONDUCTORS

A. Dielectric response function

To begin we consider a medium that is subjected to an electromagnetic field of frequency ω. So long as this material is homogeneous, isotropic, linear, and local in its response, that response may be characterized quite generally by a frequency-dependent complex dielectric function $\epsilon(\omega)$ which we write in terms of its real and imaginary parts as

$$\epsilon(\omega) = \epsilon_1(\omega) + \frac{4\pi i}{\omega}\sigma_1(\omega). \tag{1}$$

Here, the quantity $\epsilon_1(\omega)$ is called the real dielectric function whereas $\sigma_1(\omega)$ is the frequency-dependent conductivity. At zero frequency $\epsilon_1(0)$ becomes the static dielectric constant and $\sigma_1(0)$ is the ordinary dc electrical conductivity, σ_{dc}.

Other quantities, in addition to $\epsilon_1(\omega)$ and $\sigma_1(\omega)$, are often used to describe the optical properties of a material. These include the complex refractive index, $N = n + i\kappa$, the skin depth, δ, and the complex conductivity, $\sigma = \sigma_1 + i\sigma_2$. These, however, are not independent quantities, being interrelated by

$$\epsilon = N^2 = \left(\frac{c}{\omega\delta}\right)^2 = 1 + \frac{4\pi i}{\omega}\sigma.$$

Thus, for example, the real and imaginary parts of ϵ and σ are related by $\epsilon_2 = 4\pi\sigma_1/\omega$ and $\sigma_2 = \omega(1-\epsilon_1)/4\pi$. (The function σ_2 is often used in discussions of the low-frequency response of superconductors while ϵ_2 is frequently shown

for the optical properties of nonconductors.) Finally, the power absorption coefficient is given by

$$\alpha = 2\left(\frac{\omega}{c}\right)\kappa = \frac{4\pi}{c}\frac{\sigma_1(\omega)}{n}.$$

The real and imaginary parts of the complex dielectric function are related by the Kramers-Kronig relations and satisfy various sum rules.[10] The Kramers-Kronig relation relates the real dielectric function and the frequency-dependent conductivity as follows:

$$\epsilon_1(\omega) = 1 + 8\mathcal{P}\int_0^\infty \frac{\sigma_1(\omega')}{\omega'^2 - \omega^2}d\omega'. \tag{2}$$

Here, $\mathcal{P}$ means "principal part." There are similar Kramers-Kronig relations between $\sigma_1(\omega)$ and $\epsilon_1(\omega)$, n and κ, etc.

For the experimental determination of optical properties, the most important of the Kramers-Kronig relations is the one relating the phase shift upon reflection, θ, to the reflectance, R, *viz*[10]

$$\theta(\omega) = \frac{\omega}{\pi}\int_0^\infty \frac{\ln R(\omega') - \ln R(\omega)}{\omega^2 - \omega'^2}d\omega'.$$

The range of the Kramers-Kronig integral extends over all frequencies, requiring extrapolations beyond the measured frequency interval. Typically, power laws are used at high frequency, $R \sim \omega^{-p}$ with $0 \leq p \leq 4$. At low frequencies the reflectance is assumed to be constant if the sample is an insulator and to follow the Hagen-Rubens relation, $R = 1 - A\sqrt{\omega}$, if the sample is a metal.

A fundamentally important sum rule is the f-sum rule or oscillator-strength sum rule:

$$\int_0^\infty \sigma_1(\omega')d\omega' = \frac{\pi}{2}\frac{ne^2}{m} \tag{3},$$

where n is the total electron density in the material, e the electronic charge, and m the free electron mass. For cases where various types of electronic excitations are well separated in frequency, one may use a partial sum rule to determine the integrated oscillator strength:

$$N_{eff}\frac{m}{m^*} = \frac{2m}{\pi n_a e^2}\int_0^\omega \sigma_1(\omega')d\omega'.$$

Here N_{eff} is the number of effective electrons per atom, molecule, or formula unit in the solid participating in optical transitions at frequencies less than ω,

m^*/m is the ratio of their effective mass to the free electron mass, and n_a is the number density of atoms, molecules, or formula units. Because the optical plasma frequency is defined as $\omega_p^2 = 4\pi ne^2/m^*$, the partial sum rule, when applied to the low frequency spectral region dominated by free electrons, is a way to estimate the plasma frequency of the conduction electrons in a metal.

An important consequence of the oscillator-strength sum rule is that the area under the curve of $\sigma_1(\omega)$ vs. ω is a constant, independent of such factors as temperature, phase transitions, etc. Thus, for example, if σ_{dc} increases with decreasing temperature then $\sigma_1(\omega)$ must decrease at higher frequencies so as to conserve the oscillator strength. As another example, a superconductor develops an infinite (delta-function) conductivity at zero frequency; the area under this delta function is removed from $\sigma_1(\omega)$ over $0 < \omega \leq 2\Delta$ (and a little higher); here, 2Δ is the superconducting energy gap.

B. Anisotropic materials

When the material is anisotropic, as are most high T_c superconductors, the dielectric function becomes a tensor quantity. The response of the medium is well characterized by this tensor dielectric function, although when the directions of the electric field of the electromagnetic wave are not along one of the principal axes of the dielectric tensor, the wave propagation can become rather complicated, with double refraction, rotation of the plane of polarization, etc.[11,12]

Some properties of the dielectric tensor are determined by the symmetry of the crystal. For the orthorhombic crystal class into which some of the high-T_c superconductors fall, the material is biaxial, with different values for the three components of the dielectric tensor; the three principal axes are fixed along the **a**, **b**, and **c** crystallographic directions. For tetragonal crystals, the material is uniaxial, with identical values for the **a** and **b** directions and a different value for the **c**-axis.

Polarized optical measurements made with the electric field vector oriented along one of the principal axis directions will be governed by that particular component of the dielectric tensor. The Kramers-Kronig relations and sum rules discussed above will apply to that component. Clearly, measurements made for

all three polarization directions will probe all three components of the dielectric tensor.

C. Drude dielectric function

The simplest model for the dielectric function of a metal is due to Drude and Sommerfeld (see Kittel[13]). According to this model, when the electrons in a metal are subjected to an external electric field the entire Fermi surface is displaced rigidly in a direction opposite to the field (on account of the negative electronic charge) by an amount proportional to the current density. The amount of the displacement is determined by a balance between two forces: (1) the -e**E** force exerted by the electric field and (2) the relaxation of electrons towards equilibrium by elastic scattering processes, treated as a viscous damping force. The relaxation rate is $1/\tau = v_F/l$, where v_F is the Fermi velocity and l the electronic mean free path.

The scattering rate is determined by the probability of collisions between electrons and phonons (giving τ_p), impurities (τ_i), the sample surfaces (τ_d), other electrons (τ_e), etc. The scattering processes are generally independent, so that the rates add:

$$1/\tau = 1/\tau_p + 1/\tau_i + 1/\tau_d + 1/\tau_e + \cdots$$

At low frequencies and at low temperatures these scattering processes are quasielastic, with the electrons having both initial and final state energies very close to the Fermi energy. At higher frequencies, even in the limit of zero temperature, emission processes become allowed, wherein an electron absorbs a photon, simultaneously emits one or more phonons or other excitations of the crystal, and scatters, thereby relaxing the current. These Holstein[7] emission processes lead to frequency-dependent scattering rates, as discussed below. For the moment, we take $1/\tau$ to be independent of frequency.

The Drude dielectric function is

$$\epsilon(\omega) = \epsilon_\infty - \frac{\omega_p^2}{\omega^2 + i\omega/\tau}. \tag{4}$$

where ϵ_∞ is the contribution from high-energy interband processes and the atomic cores (typically $1 \leq \epsilon_\infty \leq 4$) and ω_p is the plasma frequency, defined

above. The real dielectric function, within the Drude model, is

$$\epsilon_1(\omega) = \epsilon_\infty - \frac{\omega_p^2}{\omega^2 + 1/\tau^2}. \tag{5}$$

When $\omega_p \gg 1/\tau$ (the usual case) the real dielectric function is negative for $\omega < \omega_p/\sqrt{\epsilon_\infty}$. It is this negative real dielectric function which causes the high reflectance of a metal below its plasma edge, because a negative $\epsilon_1(\omega)$ (along with $|\epsilon_1| \gg |\epsilon_2|$, i.e., $\omega \gg 1/\tau$) makes the imaginary part of the refractive index much larger than the real part, so that $N \approx i\kappa$. In turn, when $\kappa \gg n$,

$$R = \frac{(n-1)^2 + \kappa^2}{(n+1)^2 + \kappa^2} \approx 1 - \frac{2}{\omega_p \tau} \sim 1$$

At lower frequencies, $\omega \ll 1/\tau$, metals have $\kappa \approx n \gg 1$ and a Hagen-Rubens reflectance,

$$R \approx 1 - \sqrt{\frac{8\omega}{\omega_p^2 \tau}}.$$

The Drude-model frequency-dependent conductivity is

$$\sigma_1(\omega) = \frac{\omega_p^2 \tau/4\pi}{1 + \omega^2 \tau 2} \tag{6}$$

Thus, the dc conductivity is

$$\sigma_{dc} = \frac{\omega_p^2 \tau}{4\pi} = \frac{ne^2\tau}{m^*} \tag{7}.$$

The frequency dependent conductivity falls steadily from this value with a characteristic width of $1/\tau$, a frequency typically in the microwave or far infrared region of the spectrum. As a rule of thumb, most metals have plasma frequencies in the 8 eV (60,000 cm^{-1}) range and have, at 300 K, $\omega_p\tau \sim 200$. This corresponds to a conductivity of $\sigma_{dc} \sim 2 \times 10^5\ \Omega^{-1}\text{cm}^{-1}$ or a resistivity of 5 $\mu\Omega$-cm. (In this chapter equations are written in esu units throughout; the conductivity is thus in sec^{-1}. To convert to practical units, $\Omega^{-1}\text{cm}^{-1}$, divide by $30c = 9 \times 10^{11}$. For quick calculations, note that with ω_p and $1/\tau$ in cm^{-1}, the conductivity in practical units is $\sigma_{dc} = \omega_p^2\tau/60$.)

D. Frequency-dependent damping

The Drude formula for the frequency dependent conductivity is strictly applicable only at low frequency and low temperature where elastic scattering from impurities that are fixed to the lattice and quasielastic scattering from thermally generated excitations such as phonons dominate. These processes limit the lifetime of an electron and result in a conductivity function with a finite width centered at zero frequency. At higher photon frequency low lying states of the system can be excited and new, inelastic scattering processes become possible. The simple Drude formula with a constant, frequency independent, scattering rate is not valid under these circumstances.

An excitation at frequency ω can make a contribution to the optical conductivity in two different ways. Free electrons can be scattered inelastically by the excitation or the electromagnetic field can couple directly to the dipole moment of the excitation. An example of the first process is the electron-phonon interaction in ordinary metals where electrons can lose energy by creating phonons.[7,8] Interband transitions provide an example of the second process. Here the energy of the photon is used to make a transition between two eigenstates in the electronic band structure. The first process can be described by adding to the constant damping term in the Drude formula another frequency dependent term. In the second process one adds to the conductivity a direct absorption process between filled and empty states in the band structure.

Inelastic scattering in metals with a frequency dependent damping rate has been treated by a number of authors.[8,14,15,16] It is found that in order to satisfy causality an imaginary part has to be added to the damping rate which can be interpreted as a modification of the mass of the electron that enters the expression for the plasma frequency. Physically, the coupling of the excitation to the electrons changes both the real and imaginary parts of the electron self energy, and therefore both the mass and the lifetime.

One starts by rewriting the Drude dielectric function in terms of a complex damping function, also called a memory function, $G(\omega) = R(\omega) + iI(\omega)$:

$$\epsilon(\omega) = \epsilon_1 + i\epsilon_2 = -\frac{\omega_p^2}{\omega[\omega + iG(\omega)]}, \tag{8}$$

where

$$\omega_p^2 = \frac{e^2}{3\pi^2\hbar}\int v dS_F.$$

Here, dS_F is an element of area on the Fermi surface and v is the velocity of the electron. The simple Drude formula corresponds to $R(\omega) = 1/\tau$ and $I(\omega) = 0$. The quantities $R(\omega)$ and $I(\omega)$ are related by Kramers-Kronig relations, for example if $R(\omega)$ is known:

$$I(\omega) = -\frac{2\omega}{\pi}\mathcal{P}\int_0^\infty \frac{R(\omega')}{\omega'^2 - \omega^2}d\omega' \qquad (9).$$

The quantities $R(\omega)$ and $I(\omega)$ can be determined experimentally. One can solve for the frequency dependent damping τ_{eff} and the frequency dependent plasma frequency ω_{eff}^2

$$1/\tau_{eff} = -\frac{\omega\epsilon_2}{(\epsilon_1 - \epsilon_\infty)} \qquad (10)$$

and

$$\omega_{eff}^2 = -(\epsilon_1 - \epsilon_\infty)(\omega^2 + 1/\tau_{eff}^2) \qquad (11).$$

The effective damping rate, $1/\tau_{eff}$, and the effective plasma frequency, ω_{eff}^2, can also be expressed in terms of the real and imaginary parts of the memory function:

$$1/\tau_{eff} = \frac{R(\omega)}{1 - I(\omega)/\omega}, \qquad (12)$$

$$\omega_{eff}^2 = \frac{\omega_p^2}{1 - I(\omega)/\omega}. \qquad (13)$$

In this pair of equations two functions are known, the effective relaxation rate and effective plasma frequency. There are three unknown quantities, R, I and ω_p. Thus to determine I and R some additional information has to be used. Often one can estimate the plasma frequency ω_p from the sum rule for the conductivity, Eq. (3), if it is exhausted by the available spectrum:

$$\int_0^\infty \sigma_1(\omega)d\omega = \frac{\omega_p^2}{8}.$$

From the definition of the plasma frequency in terms of an effective mass m^* one can write

$$\omega_{eff}^2 = \frac{4\pi n e^2}{m^*}.$$

Then, with the definition $m^* = m/(1+\lambda)$, we find:

$$\lambda(\omega) = -I(\omega)/\omega. \tag{14}$$

The mass renormalization function λ can also be calculated from Eq. (9), the Kramers-Kronig relations between $R(\omega)$ and $I(\omega)$, if $1/\tau$ is known over a wide range of frequencies.

In summary, if the plasma frequency is known one can, from the real and imaginary parts of dielectric function, derive the frequency dependent mass and damping rate of the electrons.

There are serious problems with the application of this formalism to real systems. The first requirement is that Kramers-Kronig derived dielectric function be available for the system in the region of interest. The second, more severe, restriction is that the dielectric function should only include intraband, that is free electron processes.

E. The electron-phonon interaction

An example of frequency dependent damping is the inelastic scattering of the conduction electrons by phonons in ordinary metals, the Holstein process. The photon energy is divided between the change in kinetic energy of the electron and the phonon energy. At zero temperature the process has a definite threshold at the frequency of the phonon—at least this much energy must be delivered to the system by the photon. The expression for the damping rate is[8]

$$1/\tau(\omega) = \frac{2\pi}{\omega}\int_0^\omega \alpha^2_{tr}F(\Omega)(\omega-\Omega)d\Omega \tag{15}$$

where $\alpha^2_{tr}F(\Omega)$ is the Eliashberg function, proportional to the phonon density of states $F(\Omega)$ modified by the inclusion of a factor $(1-cos\theta)$ to weight large scattering angles θ that make a larger contribution to transport properties such as the frequency dependent conductivity.

In the superconducting state the development of the gap 2Δ at the Fermi level means that the formalism must be modified. Two important changes occur. In the normal state the threshold of the broad structure caused by the phonons occurs at a frequency Ω_E. In the superconducting state an additional energy 2Δ must be available to break the Cooper pairs. As a result this threshold shifts to

a higher frequency $\Omega_E + 2\Delta$. In addition the singularities in the superconducting density of states cause the phonon structure to sharpen. As a result an $\alpha^2 F(\Omega)$ function can be extracted from the optical spectrum with a resolution that rivals that of the familiar tunnelling method.[9]

F. Interband transitions

The general subject of interband transitions is beyond the scope of this review. Ordinary interband transitions in solids are due to excitations of electrons from one set of energy eigenstates to a higher lying set of states; they are thus governed by the details of the electronic band structure.[10] In contrast to the Drude model, which describes relatively accurately the free carrier response, the simple Lorentz oscillator commonly used to model interband transitions does a poor job of representing the lineshape. Nevertheless, this model is widely used to represent the interband and bound-carrier contributions to the dielectric function.

The Lorentzian dielectric function is easily derived in the same spirit as the Drude model by assuming that the electrons are bound by a harmonic potential to a site in the solid, and that motion in this potential is subject to a viscous damping force. The dielectric response function is then given by:

$$\epsilon(\omega) = \epsilon_\infty + \frac{\omega_{pe}^2}{\omega_e^2 - \omega^2 - i\omega\gamma_e}. \tag{16}$$

Here ϵ_∞ is as usual the high-frequency limiting value of the dielectric function and ω_{pe} plays the role of an oscillator strength or plasma frequency; it is given by $\omega_{pe} = \sqrt{4\pi n_o e^2/m^*}$, where n_o is the number density of oscillators and m^* their effective mass.

The other terms in Eq. (16) are the center frequency, ω_e, and the linewidth or damping constant, γ_e. It is tempting to associate ω_e with the semiconducting energy band gap or interband energy and γ_e with the lifetime of excited carriers. This association is valid if the width of the band is caused by lifetime effects, as in atomic absorption. If, however, the width is due to the initial and final states being located in broad bands, so that there is a large range of allowed energies for interband transitions, the association is invalid and will *overestimate* both energy gap and the lifetime. In this case, the gap should be associated with the onset of the absorption rather than with its center frequency.

There are however three features of the Lorentz oscillator which can be interpreted with confidence. First, so long as the damping is not too large there is a range of frequencies over which $\epsilon_1(\omega) < 0$. As in the case of the Drude metal, this negative $\epsilon_1(\omega)$ leads to a high "metallic" reflectance; the frequencies where this occurs are $\omega_e \leq \omega \leq \omega_{pe}\sqrt{1/\epsilon_\infty + \omega_e^2/\omega_{pe}^2}$. Second, the sum rule gives $\omega_{pe}^2/8$ for the oscillator strength of the Lorentzian. Both of these facts justify the use of the Lorentz oscillator model to represent interband transitions.

The third important feature of the Lorentz model is its zero-frequency limit:

$$\epsilon_1(0) = \epsilon_\infty + \frac{\omega_{pe}^2}{\omega_e^2} \tag{17}$$

Thus, interband transitions contribute important terms to the static dielectric constant, which increases as ω_{pe} increases or ω_e decreases. This behavior is consistent with observed behavior in semiconductors.[17]

G. Frequency-dependent conductivity of superconductors

The electromagnetic properties of superconductors are distinguished by perfect dc conductivity, the Meissner exclusion of magnetic fields, and a gap 2Δ in the electronic excitation spectrum. The gap is the minimum energy required to break apart a pair. In weak-coupling BCS theory, this energy at 0 K is given by

$$2\Delta = 3.5 k_B T_c \tag{18}$$

where k_B is Boltzmann's constant and T_c is the superconducting transition temperature. Actual superconductors do not adhere rigidly to this relation, with strong-coupled superconductors (Pb and Hg) showing $2\Delta/k_B T_c \approx 4$.

The infinite dc conductivity is represented in the frequency- dependent conductivity of a superconductor by a delta function at zero frequency. In contrast, at all non-zero frequencies below the gap the real part of the conductivity is zero at zero temperature and exponentially activated at finite temperature. With $\sigma_1(\omega) = 0$ there is no energy absorption for $0 < \omega < 2\Delta$. There is, however, a substantial inductive response of the superconductor in the low frequency range.

To see how this inductive response arises, we consider the London model. According to the London model, Ohm's law is replaced by the London equation

$$\mathbf{j}_s = -\frac{n_s e^2}{m^* c}\mathbf{A}$$

where $\mathbf{j}_s$ is the supercurrent, $\mathbf{A}$ is the magnetic vector potential and n_s is the density of superfluid carriers. (Here we take these to have charge e and mass m; the model can also be written—with identical results—in terms of Cooper pairs, with charge $-2e$, mass $2m^*$, and number density $n/2$.)

If the London equation is combined with one of Maxwell's equations, $\nabla \times \mathbf{H} = (4\pi/c)\mathbf{j}_s$, it is straightforward to show that an external magnetic field decays exponentially inside a superconductor with a characteristic length, the London penetration depth,

$$\lambda_L = \sqrt{\frac{m^* c^2}{4\pi n_s e^2}} \tag{19}$$

Note that if n_s=n, then $\omega_L \equiv c/\lambda_L = \omega_p$.

Taking the time derivative of the London equation, one finds

$$\frac{\partial \mathbf{j}_s}{\partial t} = \frac{n_s e^2}{m^*}\mathbf{E}$$

where we have used $\mathbf{E} = -\frac{1}{c}\frac{\partial \mathbf{A}}{\partial t}$. This is just another way of writing $m^*\mathbf{a}_s = -e\mathbf{E}$, where $\mathbf{a}_s$ is the superfluid acceleration and $\mathbf{j}_s = -n_s e \mathbf{v}_s$. We use $e^{-i\omega t}$ time dependences for $\mathbf{j}_s$ and $\mathbf{E}$, and find that

$$\mathbf{j}_s = i\frac{n_s e^2}{m^* \omega}\mathbf{E}$$

or (recalling that the dc conductivity is infinite):

$$\sigma(\omega) = A\delta(\omega) + i\frac{n_s e^2}{m^* \omega} = \frac{\omega[\epsilon(\omega) - 1]}{4\pi} \tag{20}$$

where A is the strength of the zero-frequency delta function in the conductivity. This can be determined by substituting $\sigma_1(\omega)$ in the Kramers-Kronig relation:

$$\epsilon_1(\omega) = 1 + 8A\int_0^\infty \frac{\delta(\omega')}{w'^2 - w^2}dw'$$

to find $A = \pi n_s e^2/2m^* = \omega_{ps}^2/8$. Thus the superfluid in the London model has a real dielectric function given by

$$\epsilon_1(\omega) = 1 - \frac{\omega_{ps}^2}{\omega^2} \tag{21}$$

This dielectric function is that of n_s free carriers, impeded by their inertia but unaffected by scattering. Similarly the frequency dependent conductivity is that of a perfect conductor,

$$\sigma_1(\omega) = \frac{\pi n_s e^2}{2m^*}\delta(\omega) = \frac{1}{8}\omega_{ps}^2\delta(\omega) \tag{22}$$

Note that this conductivity satisfies the f-sum rule if $n_s = n$ so that $\omega_{ps} = \omega_p$. Thus in the London model all of the oscillator strength of the Drude normal-state conductivity ends up under the zero-frequency delta function of the superconductor. This is a consequence of the gap in the London model effectively being infinity.

A more realistic dielectric function for a superconductor is the one developed by Mattis and Bardeen,[18] who calculated the real and imaginary parts of the frequency-dependent conductivity within weak-coupling BCS theory. The calculation is valid either in the extreme clean limit or the extreme dirty limit. Here we define these two limits as

$$\text{Clean limit :} \qquad \frac{1}{\tau} \ll 2\Delta.$$

$$\text{Dirty limit :} \qquad \frac{1}{\tau} \gg 2\Delta.$$

We set $\hbar = 1.0$. This is the key definition for optics. Because the Pippard coherence length is $\xi_0 = v_F/\pi\Delta$, the above definitions correspond respectively to $l \gg \xi_0$ in the clean limit and $l \ll \xi_0$ in the dirty limit.

Fig. 1 shows the Mattis-Bardeen theory for $\sigma_1(\omega)/\sigma_n$ and $\sigma_2(\omega)/\sigma_n$ as a function of frequency. The real part is zero up to the energy gap and then rises to join the normal-state conductivity at a substantially higher frequency. In actual metallic superconductors, this edge usually is much steeper. The imaginary part displays the $1/\omega$ inductive response discussed above.

It is important to note that Fig. 1 is somewhat misleading because it shows not the conductivity, but the ratio of the conductivity to its normal state value. In the dirty limit, σ_{1n} is nearly constant so long as $\omega \ll 1/\tau$, e.g., for $\omega \sim 2\Delta$, and the figure is a reasonable representation of σ_{1s} and σ_{2s}. Much of the Drude oscillator strength exists at frequencies above 2Δ, leading to numerical changes from the London model dielectric function discussed above. The area under the

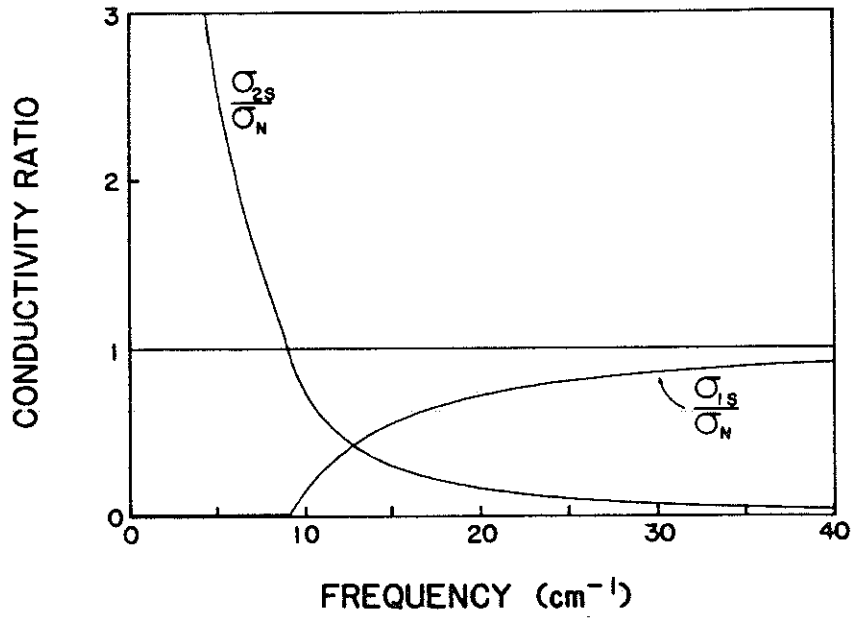

FIG. 1. Real and imaginary parts of the frequency-dependent conductivity of a superconductor, calculated from the theory of Ref. 18.

zero-frequency delta function and the prefactor in the $1/\omega^2$ term in $\epsilon_1(\omega)$ are both substantially reduced. In the dirty limit, these quantities should be multiplied by a factor approximately equal to $2\Delta\tau$, a quantity much smaller than unity.

In the clean limit, most of the area under the Drude $\sigma_1(\omega)$ is contained in the frequency range well below 2Δ. Therefore, at frequencies larger than 2Δ, σ_{1n} is extremely small compared to σ_{dc}. As a result, the London model accurately describes the infrared response, which is mostly inductive. The zero-frequency delta function contains most of the oscillator strength and the reactive response is essentially that of free carriers at all frequencies above and below 2Δ.

One model which attempts to bridge the gap between the extreme clean and extreme dirty limits is that due to Leplae,[19] who put relaxation effects into the Mattis-Bardeen theory in a plausible but not completely rigorous way. The Leplae model has been used by a number of authors, e.g., Ref. 20.

III. THE MIDINFRARED BAND

We start with a discussion of the normal-state behavior of these materials. As has been generally recognized, the high T_c superconductors have anomalous normal-state electronic properties. Among these we mention the relatively high resistivity of $YBa_2Cu_3O_{7-\delta}$ and $La_{2-x}Sr_xCuO_4$, the linear temperature dependence of the resistivity, the very wide range of temperatures over which this linear temperature dependence is observed, and the insulating behavior of compositions that should be half-filled-band metals, e.g. La_2CuO_4 and $YBa_2Cu_3O_6$.

Most measurements of the optical properties of these materials have been reflectance studies. There are not wide differences in the results of these measurements, so it would be possible to construct a generic "high-T_c" reflectance curve. Despite this general agreement about the data, a number of controversial issues have arisen, including: (1) the presence (or absence) of a midinfrared absorption band, (2) the use of the Drude model to describe the infrared reflectance, (3) interpretations of doping studies, (4) the frequency dependence of the effective mass and scattering rate, (5) the effects of anisotropy and inhomogeniety, and (6) the importance of electron-vibrational interaction. Each of these will be discussed in this section. Phonon assignments are the subject of the following chapter of this volume and will not be discussed here. We will, however, briefly touch on the high frequency bands seen in the visible and ultraviolet.

A. Early studies of ceramics

As was the case with all experimental studies of high-temperature superconductors, the first infrared measurements were made on ceramic samples — first $La_{2-x}Sr_xCuO_4$ but were followed shortly by $YBa_2Cu_3O_{7-\delta}$. The first complete infrared spectrum of a high-temperature superconductor that we know of was presented by Tajima *et al.*[21] It is shown in Fig. 2. (This spectrum was also presented at the "Woodstock" session of the March 1987 APS meeting.) The room-temperature reflectance is shown for ceramic samples of $La_{2-x}Sr_xCuO_4$ with $x = 0.18$, $La_{2-x}Ba_xCuO_4$ with $x = 0.10$, and La_2CuO_4. Note that these data are presented on a wavelength scale from 0.5 μm (20,000 cm^{-1} or 2.5 eV) to 100 μm (100 cm^{-1} or 12 meV).

There are three characteristic features of these spectra, features which occur in all subsequent spectra of ceramic samples: (1) The doped or substituted

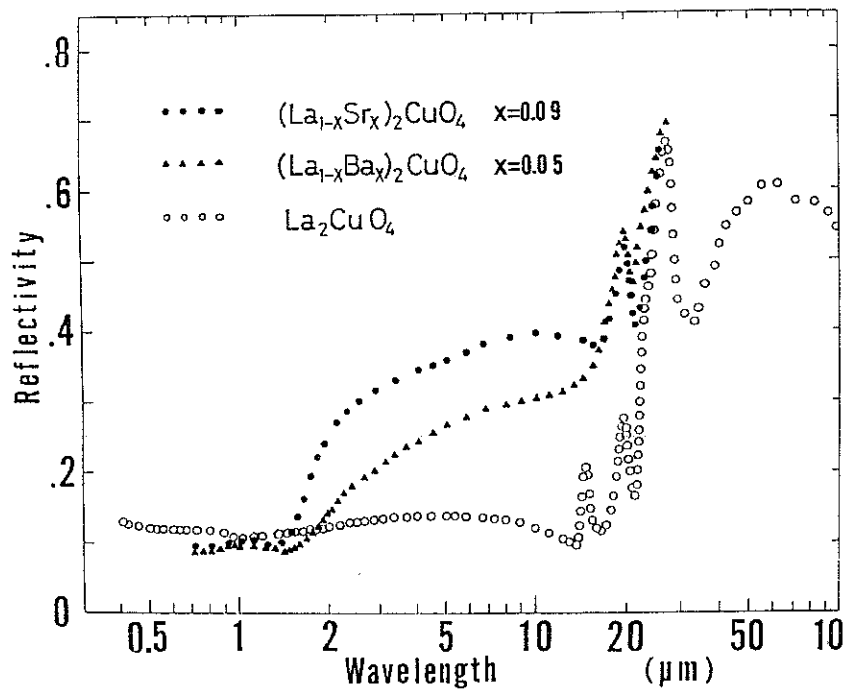

FIG. 2. Infrared reflectance of $La_{1.82}Sr_{0.18}CuO_4$, $La_{1.90}Ba_{0.10}CuO_4$, and La_2CuO_4 over 0.5–100 μ. Note that the data are presented as a function of wavelength. (From Ref. 21.)

samples have a reflectance minimum at 1.5 μ (0.83 eV), followed by a steep rise in reflectance at longer wavelengths. This feature is absent in the non-superconducting La_2CuO_4 sample. (2) The intensity of the infrared reflectance rise was strongest in the most heavily-doped sample, but the location of the reflectance minimum did not change with doping level. (3) Strong phonon features are seen in the infrared; one mode which is seen in La_2CuO_4 is absent in the doped samples. The spectra were discussed in terms of a plasma edge and metallic reflectance of free carriers by Tajima *et al.*..

Shortly afterwards, Orenstein *et al.*[22] presented room-temperature reflectance spectra of $La_{2-x}Sr_xCuO_4$ ($x = 0.175$), La_2CuO_4, and $YBa_2Cu_3O_{7-\delta}$ while Herr *et al.*[23] described the reflectance of $La_{2-x}Sr_xCuO_4$ ($x = 0.15$) at 4.2 K, 70 K, and 300 K. Both groups concluded that the optical properties deviated from those of a simple Drude metal, with a strong absorption feature located in the midinfrared and with the free-carrier (Drude) response contributing only a small part of the total infrared oscillator strength. Despite rather different analysis methods, both groups put the midinfrared feature at 0.44–0.45 eV, but with a very broad ($\sim$ 1 eV) linewidth. To reach this conclusion Orenstein *et al.*[22] fit

the reflectance of $La_{2-x}Sr_xCuO_4$ using a dielectric function model consisting of a sum of Drude and Lorentzian terms, finding that the Lorentzian part (centered near 0.4 eV) dominated the spectrum. In $YBa_2Cu_3O_{7-\delta}$ the midinfrared band was put at 0.65 eV.

Herr *et al.*[23] performed a Kramers-Kronig analysis of the reflectance to obtain the frequency-dependent conductivity, shown in Fig. 3. (Note that the 4.2 K conductivity shown in this figure is too large, on account of errors in the low temperature reflectance at high-frequencies. The actual temperature dependence is smaller than indicated here.) In addition to the midinfrared absorption, Herr *et al.*[23] concluded that the vibrational features (particularly the 240 cm^{-1} mode) were anomalously strong.

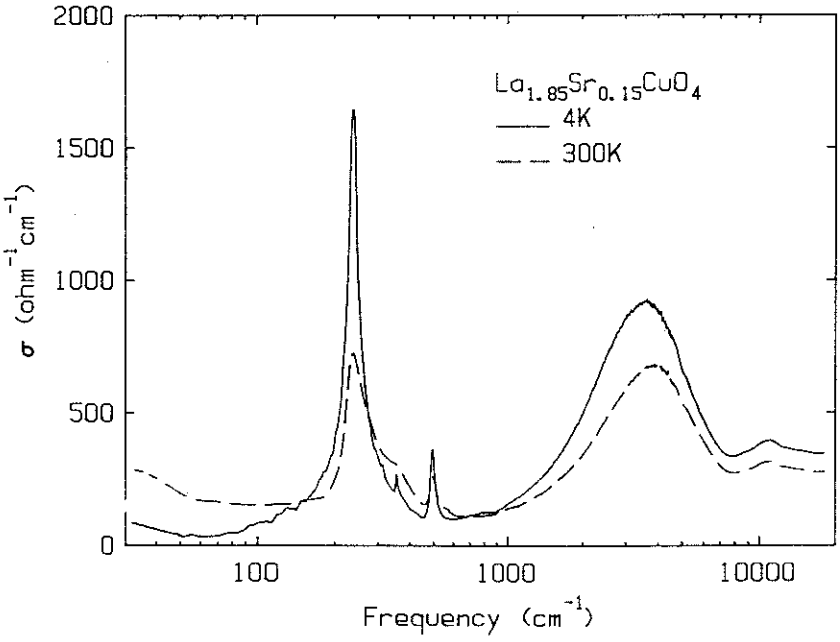

FIG. 3. Frequency-dependent conductivity of $La_{1.85}Sr_{0.15}CuO_4$, as determined by Kramers-Kronig analysis of reflectance. Note the logarithmic frequency scale. (From Ref. 23.)

The far-infrared and midinfrared properties of $YBa_2Cu_3O_{7-\delta}$ ceramic samples were described by Bonn *et al.*[24] and Kamarás *et al.*[25]. Kramers-Kronig analysis gave a broad midinfrared band near 0.37 eV, again with a width approaching 1 eV. Comparison of the spectra of superconducting $YBa_2Cu_3O_{6.9}$ and nonsuperconducting $YBa_2Cu_3O_{6.2}$ showed that the midinfrared band was present only in the former sample

The interpretation of these results attributed the midinfrared absorption to a charge-transfer electronic excitation among strongly correlated, perhaps localized electrons, of the sort proposed by Varma *et al.*[26] This "excitonic" absorption is a very controversial issue, as discussed below. It is clear that anisotropy and inhomogeniety distorted these early spectra, making the positions of the bands particularly inaccurate.[27] Nevertheless, as we argue below, it is our belief that the midinfrared oscillator strength is dominated by absorption which is due to some sort of particle-hole excitation and that only a small amount of the absorption arises from the zero-frequency-centered Drude absorption of free carriers.

In contrast, polarized data have made evident, as first pointed out by Schlesinger *et al.*,[28] that the vibrational features are not anomalously strong; instead, the mixing of **c**-axis phonon structure with **ab**-plane electronic absorption leads to an erroneous increase in the apparent oscillator strength as determined either by Kramers-Kronig analysis[23,25] or by fits to model dielectric functions.[29]

A number of workers have discussed the effects of anisotropy on the optical properties of ceramic samples, either using effective medium theories,[23,30,31,32] which should apply when the wavelength exceeds the average grain size, or by calculating an average reflectance,[28,32,33] a model which is appropriate when the wavelength is small relative to the grain size. In many ceramic samples the grain size is $\sim 10\mu$, so neither limit is strictly applicable. Qualitative agreement with spectra in the near-infrared and midinfrared regions for ceramic samples of $La_{2-x}Sr_xCuO_4$ can be obtained by taking the reflectance to be a sum of 2/3 **ab**-plane reflectance and 1/3 **c**-axis reflectance spectra.

B. The Drude fits

The reflectance of ordinary metals is dominated by a plasma edge in the visible or ultraviolet, with a rapid rise to high reflectance at longer wavelengths. This spectrum can in general be modelled by a Drude dielectric function, Eq. (4), especially if ϵ_∞ is made frequency dependent in order to describe the contributions of interband transitions. The value of ω_p then corresponds closely to the free-carrier or band-theory results for these quantities. Typical metals have $\omega_p\tau \sim 200$, making the reflectance rise at the plasma edge rather steeply. As the scattering rate increases, the width of the edge also increases. It is im-

portant to note, however, that semiconductors (e.g., Si and Ge) also display an ultraviolet plasmon edge, with high "metallic" reflectance at frequencies between the plasmon frequency and their semiconducting energy gap.[10] This is due to the negative values of $\epsilon_1(\omega)$ between the gap and the plasmon frequency. (See section II.F.)

The reflectance of the high T_c superconductors resembles that of ordinary materials in many ways,although the "plasma edge" is in the infrared. Many groups have taken the Drude model to describe the infrared properties of the high T_c superconductors, including studies of $La_{2-x}Sr_xCuO_4$ceramics,[21,28,32,34] the **ab**-plane of $La_{2-x}Sr_xCuO_4$ crystals,[35,36] $YBa_2Cu_3O_{7-\delta}$ceramics,[31,33,37] the **ab**-plane of $YBa_2Cu_3O_{7-\delta}$crystals,[27,38,39,40] and **c**-axis-normal $YBa_2Cu_3O_{7-\delta}$ thin films.[41,42]

Leaving aside for a moment the question of the applicability of the Drude model to the high T_c superconductors, we first discuss the results of these fits. Despite the wide range of samples studied, most find rather similar Drude parameters:

(1) In $La_{2-x}Sr_xCuO_4$ $\omega_p \approx$ 1.6–1.7 eV (12,800–13,700 cm^{-1}) (independent of x!), $\epsilon_\infty \approx$ 4.0–4.5, and $1/\tau \approx$ 0.37–0.60 eV (3000–5000 cm^{-1}).

(2) In $YBa_2Cu_3O_{7-\delta}$ these parameters are $\omega_p \approx$ 2.6–3.1 eV (21,000–25,000 cm^{-1}), $\epsilon_\infty \approx$ 3.7–4.5, and $1/\tau \approx$ 0.6–1.2 eV (5000–10,000 cm^{-1}).

Two examples of Drude model fits are shown in Figs. 4 and 5.

Fig. 4 (from Ref. 38) shows the room temperature reflectance and Kramers-Kronig-derived conductivity for a crystal of $YBa_2Cu_3O_{7-\delta}$. The data are shown as points, $\sigma_1(\omega)$ as a dashed curve, and the Drude model reflectance and conductivity as solid lines. The Drude parameters are ω_p = 3.1 eV (25,000 cm^{-1}), and $1/\tau$ = 0.93 eV (7500 cm^{-1}). (ϵ_∞ was not specified; from the location of the minimum in the reflectance fit, it must have been $\epsilon_\infty \sim 4$.)

Fig. 5 (from Tajima *et al.*[36]) presents the reflectance, R, the real part of the dielectric function, ϵ, the loss function, -Im$(1/\epsilon)$, and the frequency-dependent

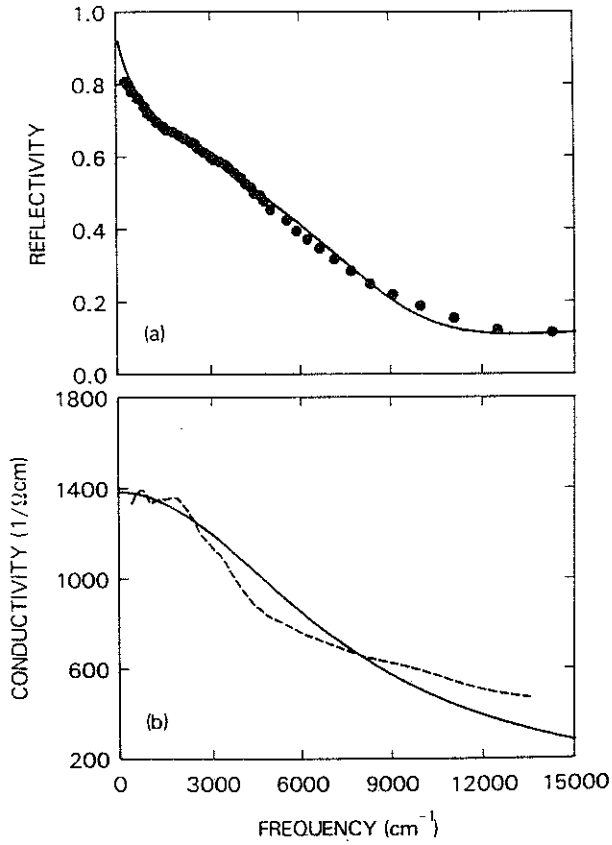

FIG. 4. The upper panel shows the room-temperature infrared reflectance of a crystal of $YBa_2Cu_3O_{7-\delta}$; the lower curve the Kramers-Kronig-derived conductivity. The solid lines are fits assuming a simple Drude dielectric function. (From Ref. 38.)

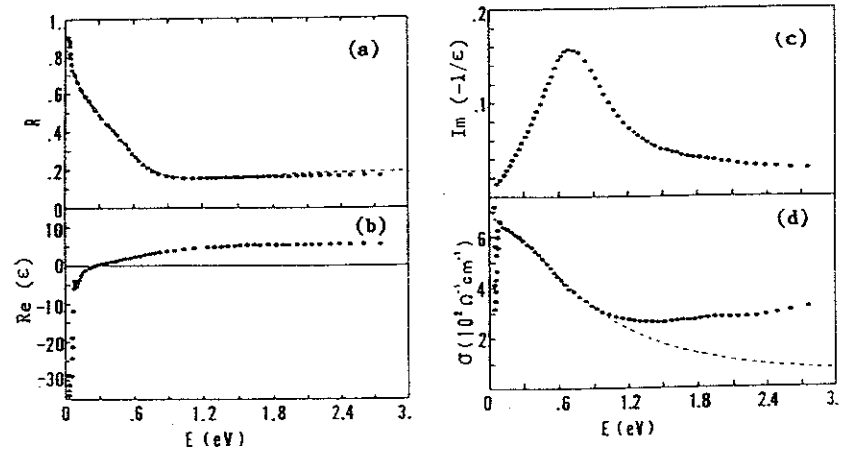

FIG. 5. The infrared room-temperature reflectance (upper left panel), real part of the dielectric function (lower left), loss function (upper right), and frequency-dependent conductivity (lower right) of of a crystal of $La_{1.8}Sr_{0.2}CuO_4$. (From Ref. 36.)

conductivity, $\sigma_1(\omega)$, of a crystal of $La_{1.8}Sr_{0.2}CuO_4$. The data, measured at 300 K, were taken with the electric field parallel to the **ab**-plane. It should be noted, however, that the superconducting transition of this sample began at $\sim$ 30 K and was not complete until $\sim$ 14 K, even though the Sr concentration of 0.2, in this ceramic, would give $T_c \approx 38$ K. Drude parameters were $\omega_p = 2.4$ eV (19,000 cm^{-1}), $\epsilon_\infty = 7$, and $1/\tau = 0.93$ eV (7500 cm^{-1}). Here, ω_p and ϵ_∞ are both somewhat larger than the typical results for $La_{2-x}Sr_xCuO_4$ quoted above; however, the screened plasmon frequency, which is $\omega_p/\sqrt{\epsilon_\infty} = 0.89$ eV in the Drude model, is very close in all samples.

The good fit of the reflectance with a Drude dielectric function was used to argue against the midinfrared absorption reported in $YBa_2Cu_3O_{7-\delta}$ ceramics by Kamarás *et al.*[25] and in $La_{2-x}Sr_xCuO_4$ ceramics by Orenstein *et al.*[22] and Herr *et al.*[23] Based on the fit shown above in Fig. 4, Schlesinger *et al.*[38] claimed that there was no evidence for a mode at 0.5 eV in their crystals. Bozovic *et al.*[42] measured the reflectance and transmittance of an oriented $YBa_2Cu_3O_{7-\delta}$ film (**c**-axis normal to the film surface), evidently in a search for narrow, semiconductor-like, excitonic lines. Not finding any, they concluded that the reflectance spectrum could be well fit with a simple Drude model.

The Drude dielectric function is characterized by a mode at zero frequency, of oscillator strength $\omega_p^2/8$, proportional to carrier concentration, broadened to $1/\tau$ by scattering processes. Considerable evidence exists against the applicability of this model to the high T_c superconductors and in favor of a strong *non-Drude* absorption in the mid infrared.[43] In the Drude model, the same scattering rate applies to both dc transport and high-frequency absorption. This is inconsistent with the known temperature dependence of the dc resistivity and midinfrared reflectance. The dc resistivity of many samples follows[44,45] $\rho = \rho_0 + aT$. This linear temperature dependence has been shown[45] to extend from T_c to 1000 K in $La_{2-x}Sr_xCuO_4$ and up to 600 K in $YBa_2Cu_3O_{7-\delta}$. In the best samples, $\rho_0 \approx 0$. In contrast, the midinfrared reflectance is essentially temperature independent. This is illustrated in Fig. 6, which shows the reflectance of a ceramic sample of $YBa_2Cu_3O_{7-\delta}$ at 55 K, 105 K, and 300 K. The lack of temperature dependence is evident.

The magnitude of both the plasma frequency and the scattering rate ob-

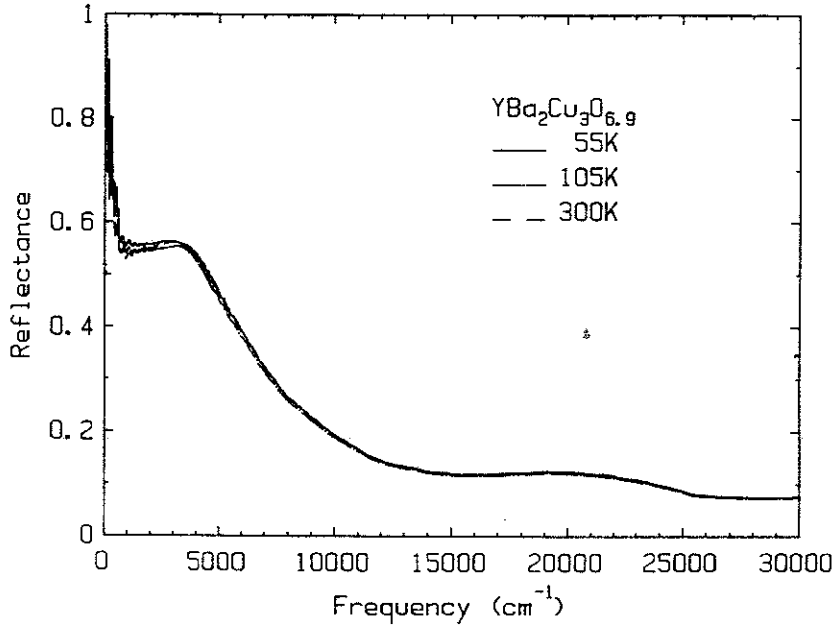

FIG. 6. The infrared reflectance of a $YBa_2Cu_3O_{7-\delta}$ ceramic sample at 55 K, 105 K, and 300 K. (From Ref. 46.)

tained by fits to the Drude model are unreasonably large. The London penetration depth, measured by muon spin resonance[47,48] or other techniques,[49] gives $\omega_p \approx 1.1$ eV in $YBa_2Cu_3O_{7-\delta}$ and $\omega_p \approx 0.6$ eV in $La_{2-x}Sr_xCuO_4$, i.e., approximately 40 % of the Drude-model result. The relaxation rate of 0.4–1.2 eV found by *all* Drude-model fits corresponds to a relaxation time of $\tau \sim 0.5$–1.5×10^{-15} sec. In turn, taking $v_F = 2 \times 10^7$ cm/sec, the mean free path would be $l = v_F\tau = 1$–3 Å. This unphysically short value for l is by itself inconsistent with the strong temperature dependence of the conductivity.[45]

Other evidence against the simple Drude model comes from studies of the optical properties as a function of Sr or Ba doping levels in $La_{2-x}Sr_xCuO_4$ and $La_{2-x}Ba_xCuO_4$, and from detailed fits to the reflectance or conductivity at a variety of temperatures. These experiments are discussed in the following subsections.

It should be pointed out that the shortcomings of the simple Drude model are only clear when low-frequency and low-temperature measurements are made; at 300 K over the range 0.1–2 eV the Drude dielectric function gives a reasonably good reproduction of the measured dielectric function. Furthermore, the Drude model dc conductivity is $\sim 1200\ \Omega^{-1}\text{cm}^{-1}$ for

$YBa_2Cu_3O_{7-\delta}$, not far from the actual room-temperature dc conductivity. Finally, the free carrier concentration estimated from the plasma frequency agrees rather well with simple estimates for the hole concentration, taking the carrier mass equal to the free electron mass:

(1) In the case of $La_{2-x}Sr_xCuO_4$, a plasma frequency of approximately 13,000 cm^{-1} gives $n = 1.6 \times 10^{21}$ $cm^{-3} \approx 0.15 n_{CuO_2}$.

(2) For $YBa_2Cu_3O_{7-\delta}$, with $\delta \sim 0$, a plasma frequency of 24,000 cm^{-1} gives $n = 5.6 \times 10^{21}$ $cm^{-3} \approx 0.5 n_{CuO_2}$.

Here, n_{CuO_2} is the number density of two-dimensional (plane) CuO_2 units in the material. As discussed below, the simple Drude-model plasma frequency is related to the integrated oscillator strength of both the far-infrared Drude and midinfrared Lorentzian contributions to the dielectric function.

C. Doping studies

Tajima *et al.*[21] observed that the location of the 0.83 eV (6600 cm^{-1}) plasmon minimum of $La_{2-x}Ba_xCuO_4$ was independent of the Ba concentration x over a range $0.06 \leq x \leq 0.18$. Similar observations have been made by several other groups.[34,39,50,51,52] The most complete study, by Etemad and coworkers,[50,51,52] covered the concentration range $0 < x \leq 0.30$ in $La_{2-x}Sr_xCuO_4$. The results are shown in Fig. 7. Even though the low frequency reflectance changes with doping level, the location of the reflectance minimum is "pinned" at 0.9 eV.

This invariance of the plasmon frequency is inconsistent with the Drude model, for which $\omega_p \sim \sqrt{n}$. It is generally assumed that the carrier concentration in $La_{2-x}Sr_xCuO_4$ equals the Sr concentration x for $x < 0.18$, and increases more slowly with x at higher doping levels on account of partial compensation by oxygen vacancies.[53] (The early argument put forth by Tajima *et al.*,[21] that the system is a tight-binding metal near the half-filled limit, making the plasma frequency nearly independent of x, has been ruled out by the observation that La_2CuO_4 is an antiferromagnetic insulator.) Even if the change above $x = 0.18$ were minimal, a change by a factor greater than 2 should have been observed if the material were described by a Drude model. It seems to us that this conclusion is valid even if the relaxation rate and effective mass are frequency dependent.

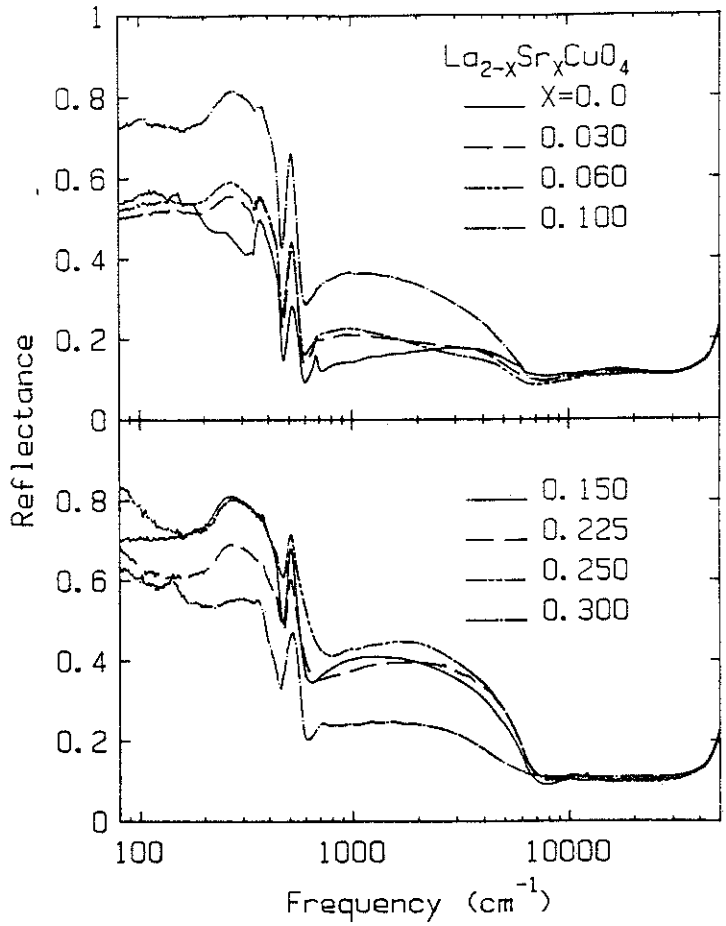

FIG. 7. Reflectance of La_2CuO_4 and $La_{2-x}Sr_xCuO_4$ at Sr concentrations between 0.02 and 0.30. The reflectance minimum at 0.9 eV is independent of Sr concentration. (From Ref. 52.)

More interesting than the pinned plasma frequency is the correlation between the intensity of the infrared absorption and the occurrence of superconductivity. This correlation, observed in $YBa_2Cu_3O_{7-\delta}$ by Kamarás *et al.*[25,54] and in $La_{2-x}Sr_xCuO_4$ by Orenstein *et al.*[39] and by Etemad and coworkers,[50,51,52] is illustrated by Fig. 8, which shows the concentration dependence of the transition temperature and the Meissner susceptibility in its upper panel and the infrared oscillator strength in its lower panel. Two measures of the oscillator strength are shown: the open circles are from the oscillator strength sum rule evaluated over the entire range below the plasmon minimum. The second (asterisks) show the apparent intensity of the c-axis polarized 240 cm^{-1} phonon of La_2CuO_4. In ceramics this intensity appears enhanced

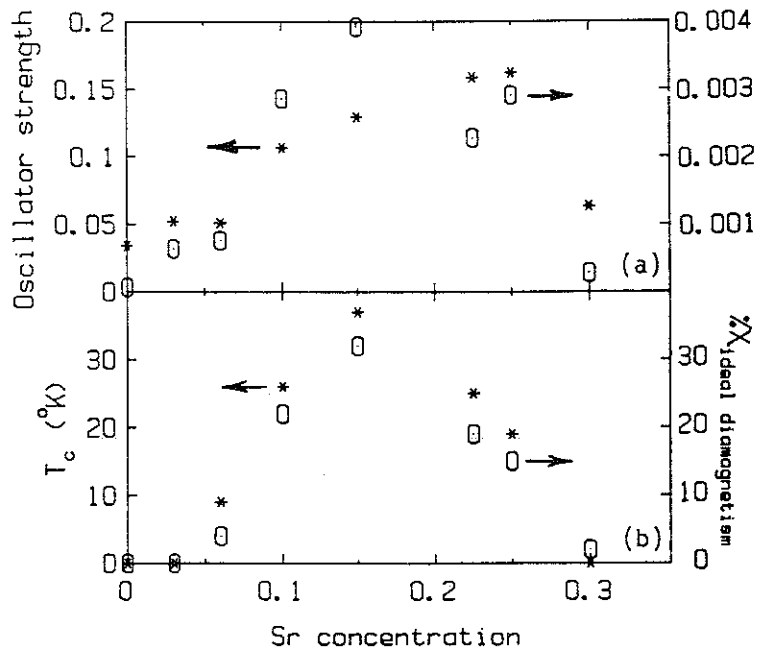

FIG. 8. Concentration dependence of superconductivity and infrared oscillator strength in $La_{2-x}Sr_xCuO_4$. The upper panel shows the infrared oscillator strength (see text); the lower the transition temperature (open triangles) and Meissner susceptibility (closed triangles). (From Ref. 52.)

because of the growth of the Drude and midinfrared **ab**-plane electronic absorption. All of the quantities plotted in Fig. 8 are seen initially to increase as the dopant concentration increases, to reach a maximum at $x \approx 0.18$ and to decrease at higher concentrations. Thus, a clear correlation exists between superconductivity and the infrared absorption.

Note that the normal-state dc conductivity is *not* correlated with the superconductivity. At high Sr concentrations, σ_{dc} continues to increase with x,[55] whereas the transition temperature, Meissner susceptibility, and the infrared oscillator strength all decrease.

D. The midinfrared absorption—textured ceramics

Several recent studies have shown that the infrared dielectric function of the high T_c superconductors may be modelled with a sum of a Drude part (governing the far-infrared properties) and a broad electronic absorption band (dominating the midinfrared properties). These studies are discussed in this and the following subsection.

The properties of "textured" ceramic samples have been discussed in detail by the McMaster–Florida group. Bonn *et al.*[56] showed that the surfaces of as-prepared ceramic samples can have a high degree of orientation, with the crystallographic **c**-axis normal to the surface of the ceramic sample. In order to achieve this texture, the ceramic pellets have to be of high density, must be annealed at high temperatures for sufficient time, and must *not* be polished or mechanically worked in any way. If these conditions are met, then x-ray and electron microscope analysis shows that approximately 80 % of the surface is covered with small crystals having their **c**-axes oriented normal to the surface. Although the surfaces are rather rough and therefore appear to be of lower optical quality than well-polished ceramic samples, It was shown[56] that the textured samples have much larger far-infrared reflectance (corrected for scattering) than do polished samples.

Optical studies on these textured samples have been made[56,57,58,59,60,61] over a wide range of frequencies and at temperatures between 2 K and 300 K. Fig. 9 shows the conductivity (determined from a Kramers-Kronig analysis of reflectance) at 100 K. Note that the conductivity has a narrow peak at low frequencies, six sharp lines (attributed to phonons), and a broad wing to high frequencies. The normal-state data cannot be fit with a simple Drude model alone; instead, a dielectric function which is a sum of Drude, (Eq. 4), Lorentzian, (Eq. 16), phonon, and high-frequency terms must be used:

$$\epsilon(\omega) = -\frac{\omega_{pD}^2}{\omega^2 + i\omega/\tau} + \frac{\omega_{pe}^2}{\omega_e^2 - \omega^2 - i\omega\gamma_e} + \sum_{j=1,N} \frac{S_j\omega_j^2}{\omega_j^2 - \omega^2 - i\omega\gamma_j} + \epsilon_\infty \qquad (23)$$

There are four contributions to this dielectric function:

(1) Drude, characterized by a plasma frequency $\omega_{pD} = 0.74$ eV (5900 cm^{-1}) and a relaxation rate $1/\tau = 0.037$ eV (300 cm^{-1});

(2) midinfrared, having a strength $\omega_{pe} = 2.6$ eV (21,000 cm^{-1}), a center frequency $\omega_e = 0.26$ eV (2100 cm^{-1}), and a width $\gamma_e = 1$ eV (8400 cm^{-1});

(3) a high frequency part, with a constant $\epsilon_\infty = 3.8$; and

(4) the phonons, represented by $N = 6$ sharp oscillators. (For the parameters of these phonon modes, see Ref. 56.)

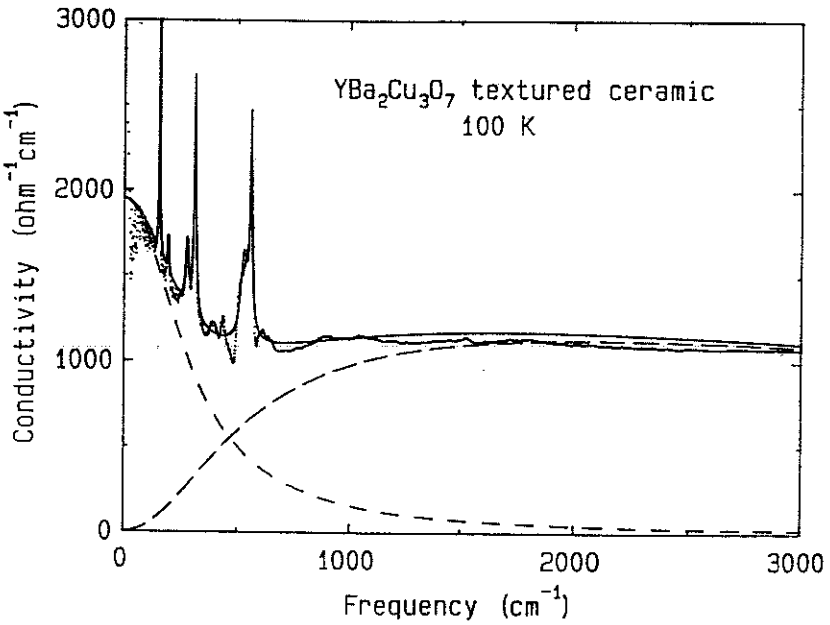

FIG. 9. Optical conductivity at 100 K of a textured ceramic sample of $YBa_2Cu_3O_{7-\delta}$. Data are shown as points while the fit to the model dielectric function of Eq. (23), which includes a Drude low-frequency part, a midinfrared band, and sharp phonons, is shown as the smooth curve. The individual contributions to $\sigma_1(\omega)$ of the Drude and midinfrared terms are shown as the dashed lines. (From Ref. 59.)

The fit to Eq. (23) is shown as the smooth curve in Fig. 9. The contribution of the Drude and the midinfrared parts are shown as the dashed lines. Although the Lorentzian representation of the midinfrared part is centered at 0.26 eV, the band has a relatively rapid onset, becoming dominant at $\sim$ 500 cm^{-1} (0.06 eV). Note that the total infrared oscillator strength is given by $\omega_p^2 = \omega_{pD}^2 + \omega_{pe}^2$, with ω_p the plasma frequency found by fits of the Drude model alone to infrared data; also, γ_e equals the relaxation rates found in such fits.

The zero-frequency intercept of the conductivity is $\sim$ 2000 Ω^{-1}cm^{-1}, somewhat below the measured 100 K conductivity, $\sigma_{dc} \approx$ 3000 Ω^{-1}cm^{-1}. Despite this discrepancy, the temperature dependence of the infrared conductivity is in *excellent* agreement with the temperature dependence of the dc resistivity. This is illustrated in Fig. 10, where the main part shows the infrared $\sigma_1(\omega)$ at three temperatures. The strongest temperature dependence is in the far infrared, with a substantially weaker high frequency behavior. The inset shows the resistivity

measured in the far infrared; the resistivity is the reciprocal of the 100 cm^{-1} conductivity. The resistivity follows the well-known[44,45] linear behavior of high-quality samples: $\rho = \rho_0 + aT$, with a relatively low value of ρ_0.

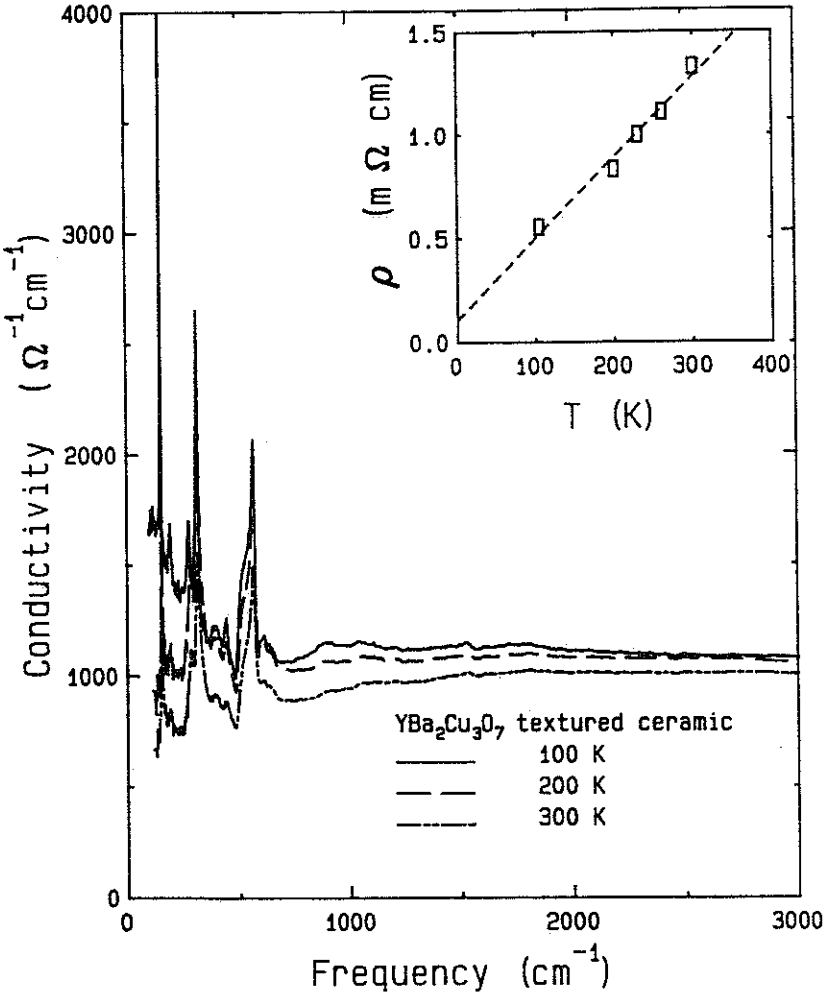

FIG. 10. Optical conductivity at 100, 200, and 300 K of a textured ceramic sample of $YBa_2Cu_3O_{7-\delta}$. The inset shows the temperature dependence of the resistivity measured by far-infrared means: the inverse of the 100 cm^{-1} conductivity. (From Ref. 59.)

Fig. 11 shows $\epsilon_1(\omega)$ at 100 and 300 K. Note that $\epsilon_1(\omega)$ is negative at low frequencies (as appropriate for a conductor) but then rises and is nearly zero above about 800 cm^{-1} (0.1 eV). (At 300 K, $\epsilon_1(\omega)$ becomes positive for a range of frequencies 800 $cm^{-1} < \omega <$ 2000 cm^{-1} whereas at 100 K $\epsilon_1(\omega)$ is negative but small in magnitude over this frequency region. It is this drop to a near zero value in $\epsilon_1(\omega)$ which causes the reflectance to display a plasmon-like drop in the

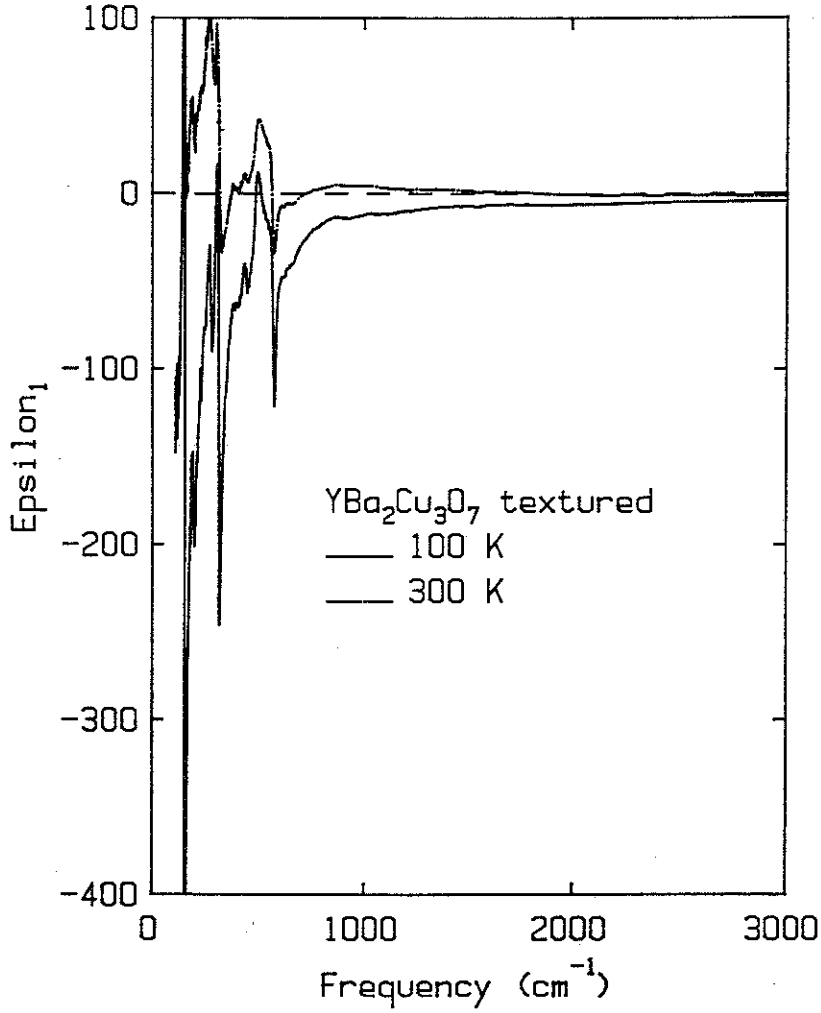

FIG. 11. Real part of the frequency-dependent dielectric function at 100 and 300 K of a textured ceramic sample of $YBa_2Cu_3O_{7-\delta}$. (From Ref. 60.)

far infrared, as discussed in section IV.

In the superconducting state, the optical properties are consistent with the Drude contribution collapsing to a delta-function at the origin, but with only minimal changes in the other parts of $\epsilon(\omega)$. As discussed by Timusk *et al.*[59] and Tanner *et al.*[60] the dielectric function is then well described by:

$$\epsilon(\omega) = -\frac{\omega_{ps}^2}{\omega^2} + i\frac{\pi\omega_{ps}^2}{2\omega}\delta(\omega) + \frac{\omega_{pe}^2}{\omega_e^2 - \omega^2 - i\omega\gamma_e} + \sum_{j=1,N}\frac{S_j\omega_j^2}{\omega_j^2 - \omega^2 - i\omega\gamma_j} + \epsilon_\infty \quad (24)$$

Here, ω_{ps} is the plasma frequency or oscillator strength of the superfluid electrons, and is proportional to $\sqrt{n_s}$, where n_s is the superfluid electron density. In the clean limit, $n_s \approx n$. (See section IV of this review) The Drude contri-

bution appropriate to the normal state has been replaced in Eq. (24) by the London-model contribution from the superconducting electrons, Eqs. (20)–(22). The first represents the inertial response at finite frequency while the second is the delta function conductivity of the superconductor. The remaining terms in Eq. (24) are the same as in Eq. (23). Most importantly, the onset of the midinfrared absorption does *not* shift to higher frequencies on entering the superconducting state. See Fig. 19 for the conductivity of the textured ceramic sample below T_c.

E. The midinfrared absorption—crystals and films

The midinfrared absorption band is also evident in the **ab**-plane infrared properties of $YBa_2Cu_3O_{7-\delta}$ crystals[57,58,59,62,63] and thin films.[60,64]

For $YBa_2Cu_3O_{7-\delta}$ the reflectance of crystal samples can be well described by Eq. (23) above T_c. The fitting parameters differ somewhat for crystal samples, but in an understandable way. At 100 K, the McMaster-Florida experiments[57,58,59] find:

(1) a Drude contribution characterized by a plasma frequency $\omega_{pD} = 1.2$ eV (9,700 cm^{-1}) and relaxation rate $1/\tau = 0.03$ eV (240 cm^{-1});

(2) a midinfrared part having a strength $\omega_{pe} = 2.5$ eV (20,000 cm^{-1}), a center frequency $\omega_e = 0.25$ eV (2000 cm^{-1}), and a width $\gamma_e = 0.6$ eV (5000 cm^{-1}); and

(3) a high frequency part modelled by a constant $\epsilon_\infty = 3.8$.

Phonon modes can be discerned in the reflectance but, on account of the substantially higher conductivity of the crystals (and somewhat lower signal-to-noise ratio of the data), phonon parameters have not been extracted.

The dc conductivity calculated from the Drude contribution to the dielectric function at 100 K gives a dc conductivity $\sigma_{dc} = 6500\ \Omega^{-1}cm^{-1}$, and agrees with the measured dc conductivity. In comparison to the textured ceramics, the crystals have a considerably higher Drude plasma frequency ω_{pD} and a slightly lower scattering rate $1/\tau$. The higher plasma frequency can be qualitatively understood in terms of a greater degree of orientation of the surface of the crystal samples.

The crystals used in the AT&T Bell Labs experiments,[62,63] had a depressed transition temperature of $T_c = 50$ K. The data were fit using Eq. (23) for the dielectric function; the results were very similar to the McMaster-Florida parameters, finding at 100 K,

(1) a Drude contribution characterized by a plasma frequency $\omega_{pD} = 1.0$ eV (8200 cm^{-1}) and relaxation rate $1/\tau = 0.015$ eV (120 cm^{-1}); and

(2) the midinfrared part having a strength $\omega_{pe} = 3.0$ eV (24,000 cm^{-1}), center frequency $\omega_e = 0.2$ eV (1700 cm^{-1}), and width $\gamma_e = 0.9$ eV (7500 cm^{-1}).

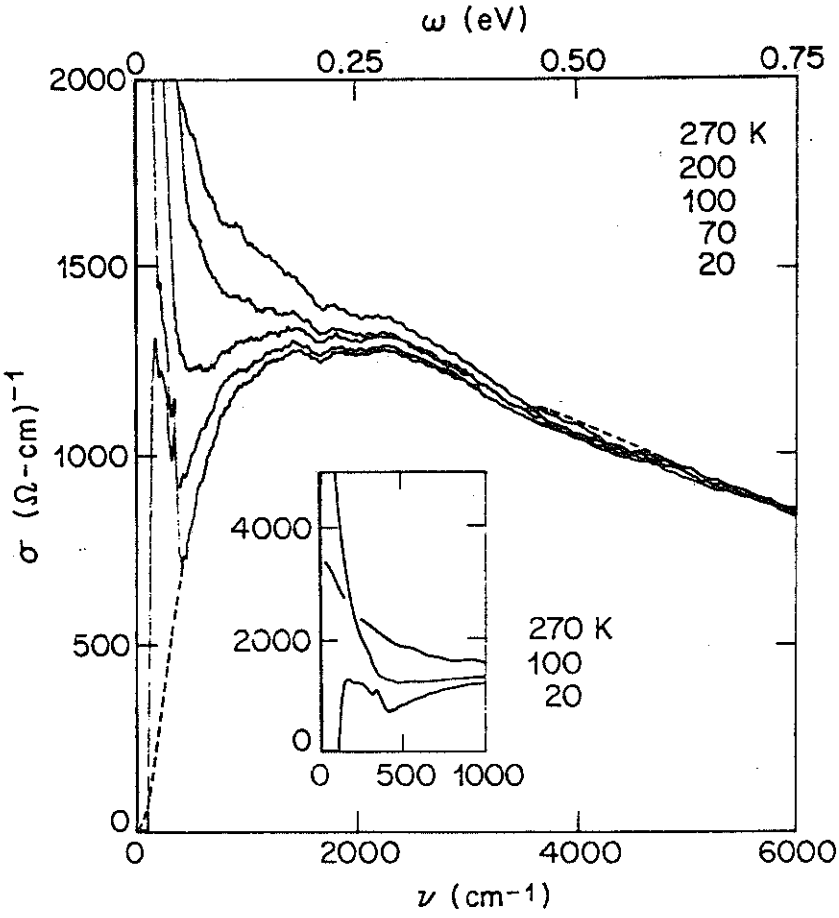

FIG. 12. Optical conductivity at five temperatures of a crystal of $YBa_2Cu_3O_{7-\delta}$ having a transition temperature of 50 K. Data are shown as lines while the midinfrared contribution to the fit is shown as the dashed line. (From Ref. 63.)

While some phonon modes can be seen, they were not included in the fit. The conductivity spectra are shown in Fig. 12 at five temperatures; the midinfrared

part of the conductivity is the dashed line. The inset shows the low frequency conductivity on a compressed scale. The data were interpreted in terms of a frequency-dependent relaxation rate and effective mass, as discussed below.

Van der Marel *et al.*[64] studied the room temperature reflectance of a thin film of $YBa_2Cu_3O_{7-\delta}$ in combination with XPS and BIS (inverse photoemission) to determine the densities of occupied and unoccupied states. Their results are shown in Fig. 13. The conductivity shows a clear peak at 0.4 eV, with additional bands at 1.4 and 2.3 eV. The convolution of the XPS and BIS spectra, which to first order corresponds to an experimentally determined joint density of states, is also shown. This function has an onset between 2 and 3 eV with a rapid rise above 4 eV. Thus the low-energy bands cannot be due to ordinary interband transitions. Van der Marel *et al.*[64] speculate that they could indicate either charge transfer (O $\rightarrow$ Cu) or a forbidden transition of Cu.

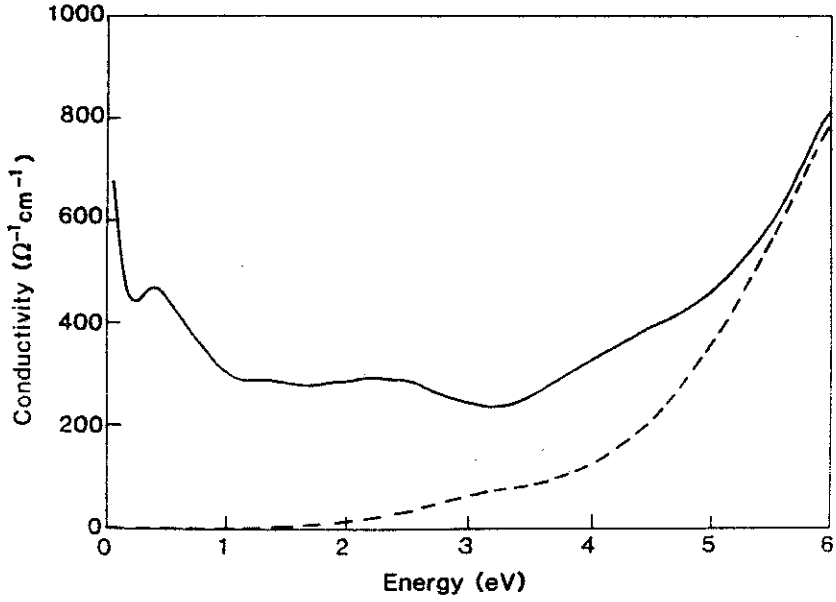

FIG. 13. Optical conductivity at room temperature of a $YBa_2Cu_3O_{7-\delta}$ thin film. The conductivity is shown as the solid line, while the joint density of states calculated from a convolution of XPS and BIS spectra is the dashed line. (From Ref. 64.)

Further independent evidence for a midinfrared absorption band comes from the *single-domain* reflectance of a crystal of $EuBa_2Cu_3O_{7-\delta}$ presented by Tanaka *et al.*[65,66], shown in Figs. 14–16. All other measurements in the 1–2–3 system are only averages over the **ab**-plane, on account of the well-known

twinning of crystals of these high T_c superconductors. (On account of this twinning, the phrase "single crystal" should in general be avoided in discussing experiments on the orthorhombic compounds, as twinned crystals are not single crystals.)

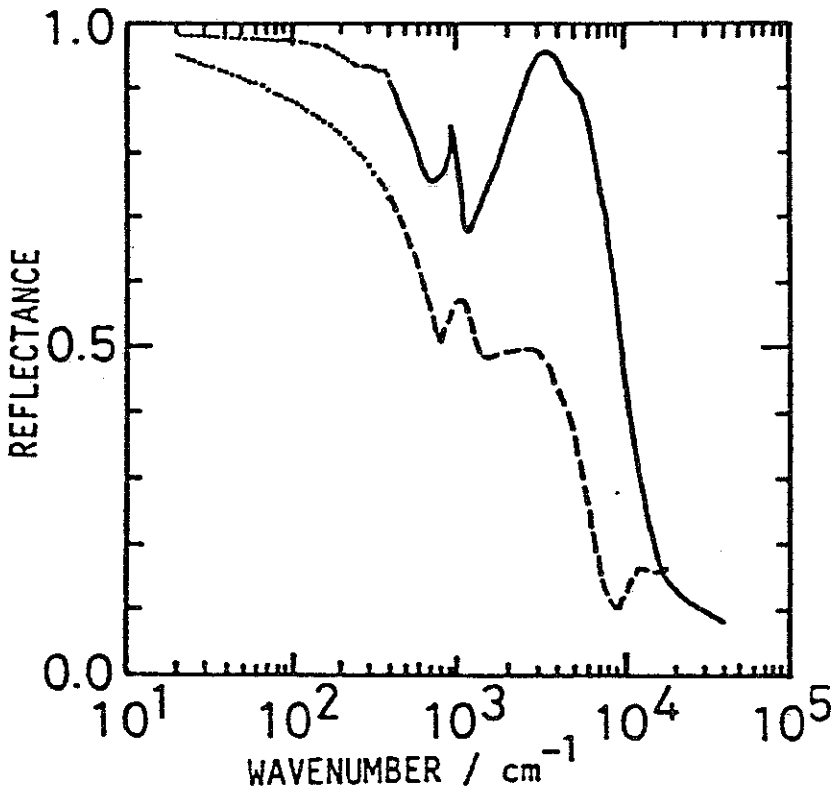

FIG. 14. Room-temperature reflectance of a *single domain* of $EuBa_2Cu_3O_{7-\delta}$. Polarization parallel to the **b** axis (i.e., the chains) is shown as the solid line while the **a**-axis polarization is shown as the dashed line. (From Ref. 65.)

Tanaka *et al.*[65,66] used a microscope to isolate a single domain on their $EuBa_2Cu_3O_{7-\delta}$ crystal, and then made polarized measurements parallel to both the **a** and **b** crystal axes. These are thus the first measurements of a single component of the dielectric tensor in the **a**- or **b**-direction. The reflectance is shown in Fig. 14. It is very interesting that these measurements show rather different spectra for the **a**-axis and **b**-axis polarizations. With the electric field along **b**, i.e., the direction of the one-dimensional Cu-O chains, the reflectance is considerably higher and the plasmon edge is both higher in frequency and sharper than for the **a**-axis polarization. Considerable structure is seen in the

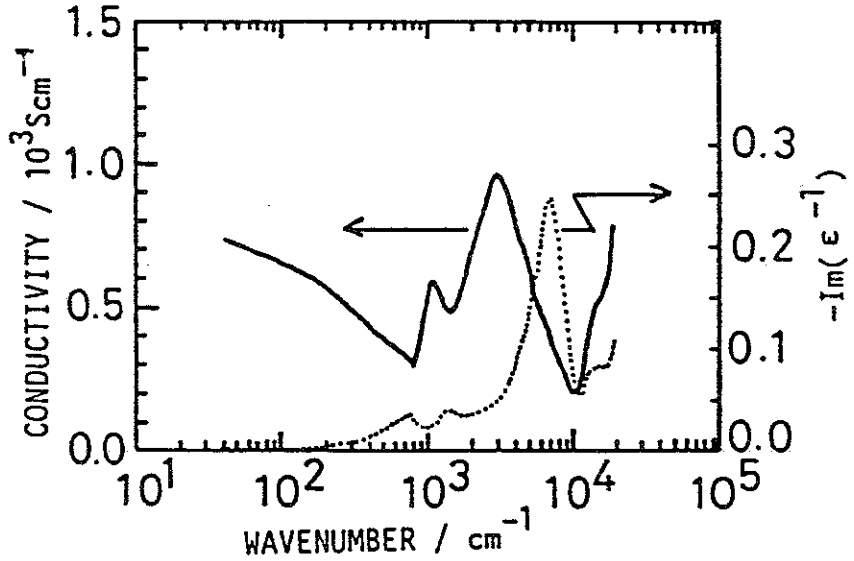

FIG. 15. Frequency-dependent conductivity (solid line) and loss function (dashed line) for the a axis of a *single domain* of $EuBa_2Cu_3O_{7-\delta}$. (From Ref. 65.)

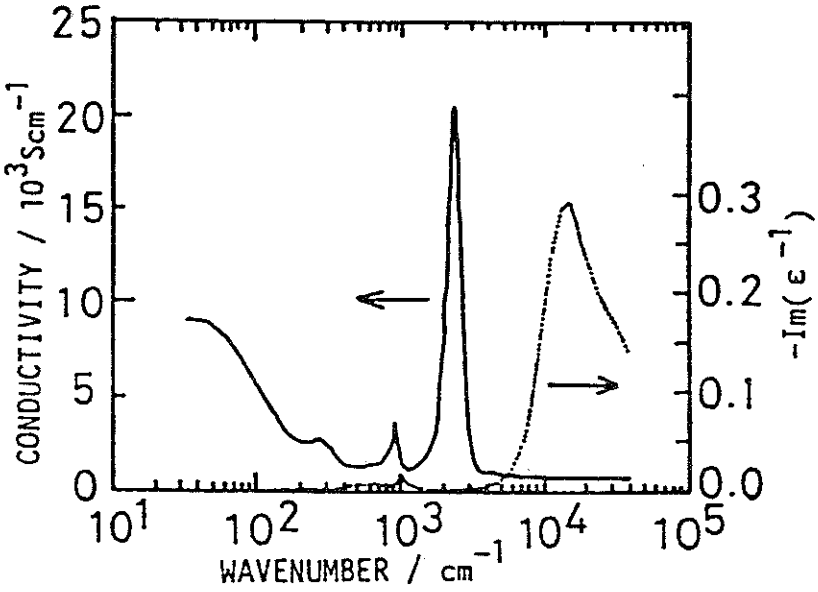

FIG. 16. Frequency-dependent conductivity (solid line) and loss function (dashed line) for the b axis of a *single domain* of $EuBa_2Cu_3O_{7-\delta}$. (From Ref. 65.)

400–2000 cm^{-1} region.

Kramers-Kronig analysis reveals that there are strong midinfrared bands in both polarizations, particularly for E $\|$ b. These are shown in Figs. 15 and 16. These figures give the conductivity, $\sigma_1(\omega)$ and loss function $-Im(1/\epsilon)$ for both polarizations. The peak in the b axis polarization is especially noteworthy.

This very intense band is located at 0.3 eV (2200 cm^{-1}) and has a width smaller than 0.1 eV (800 cm^{-1}).

Evidence of a strong midinfrared absorption has also been seen in studies of La_2CuO_4 crystals[67] and $La_{2-x}Sr_xCuO_4$ films.[68] Gervais *et al.*[67] expanded on the beautiful polarized measurements of La_2NiO_4 single crystals presented by Bassat *et al.*,[69] which demonstrated the strong anisotropy in both the electronic and vibrational contributions to the optical properties of that material. From their analysis they concluded that an electronic mode, polarized in the **ab** plane occurs both in La_2NiO_4 and $La_{2-x}Sr_xCuO_4$.

F. Frequency-dependent scattering and effective mass

Thomas *et al.*[63] and Collins *et al.*[70] have recently presented an alternative to the decomposition of the dielectric function into a sum of Drude and midinfrared bands: use of a frequency-dependent scattering rate, $\Gamma(\omega)$, and effective mass, $m^*(\omega)$. (For a discussion of the use of $\Gamma(\omega)$ and $m^*(\omega)$ in the Drude formula, see subsection II.D of this review.) The application of this formalism gives an effective mass which is close to the free electron mass at high frequencies and which becomes an order of magnitude larger at low frequencies. Note that the high-frequency value for the effective mass is based on the assumption that the carrier concentration is $\sim 6 \times 10^{21}$ cm^{-3}. (See the discussion in section III.B above.)

The scattering rate is large and nearly temperature independent at high frequencies: $\Gamma(\omega) \approx 0.9$ eV (7000 cm^{-1}) for $\omega > 0.25$ eV (2000 cm^{-1}). At low frequencies, the rate becomes smaller and strongly temperature dependent; Thomas *et al.*[63] find $\Gamma(0)$ varying from 0.4 eV (3200 cm^{-1}) at room temperature to 0.12 eV (1000 cm^{-1}) at 100 K. Not surprisingly, these high- and low-frequency limiting values are comparable to the corresponding midinfrared band and far-infrared Drude contributions to the dielectric function, as described in subsection III.E of this review. The scattering rate values differ because Thomas *et al.*[63] have defined the scattering rate so that $\Gamma(\omega) = [m^*(\omega)/m][1/\tau(\omega)]$.

The changeover from low to high-frequency behavior occurs between 0.03–0.1 eV (250–800 cm^{-1}). This is taken[63,70] to suggest that the electrons are strongly coupled ($\lambda \approx 9$) to a set of excitations which occur in this approximate

energy range. The frequency-dependent scattering rate and mass are interpreted as due to the Holstein effect,[7] in which a carrier can absorb a photon of energy ω, emit an excitation of energy $\mathcal{E}$ and scatter, so long as $\omega > \mathcal{E}$. This phenomenon leads to an enhanced scattering rate at high frequencies, as discussed in subsection II.D of this review.

There are two observations in the high T_c superconductors which work against this explanation. First, if the increase in scattering rate is due to the Holstein effect, and if the high T_c superconductors have a superconducting energy gap, then the midinfrared band should shift upwards by 2Δ in the superconducting state. The reason for the shift is straightforward: in the superconducting state the absorbed photon must have sufficient energy to break a pair as well as create the excitation. In the high T_c superconductors no upshift is seen. Fig. 12 shows that the edge of the mid infrared band is at the same location in the superconducting and normal state.

Second, any excitation which is strongly coupled to the conduction carriers will affect the dc conductivity once temperature is high enough to thermally populate the excitation spectrum, e.g., once $k_BT \sim \mathcal{E}$. One therefore expects to see a significant modification of the temperature dependence of the conductivity at $T \geq 350$ K. In the high T_c superconductors no change in the temperature coefficient occurs at these temperatures,[45] suggesting that excitations in this energy range do not contribute to the scattering of conduction carriers.

G. High frequency bands

A number of authors have studied the high-frequency (> 1 eV) properties of $La_{2-x}Sr_xCuO_4$ ceramics[23,50], $La_{2-x}Sr_xCuO_4$ crystals[35], $YBa_2Cu_3O_{7-\delta}$ ceramics,[25,46,71,72] $YBa_2Cu_3O_{7-\delta}$ films,[64,73] and $YBa_2Cu_3O_{7-\delta}$ crystals.[72] A number of electronic bands are seen, some of which have interesting dependences on x or δ, whereas others are present at all concentrations of Sr or O.

The concentration-independent bands in $La_{2-x}Sr_xCuO_4$ occur at 1.4, 2.7, and 5 eV, with the 5 eV feature being the onset of strong interband absorption. $YBa_2Cu_3O_{7-\delta}$ has absorptions at 2.5–2.7 eV and above 6 eV, with the latter energy corresponding to the onset of strong interband transitions.

Etemad *et al.*[50] studied the Sr concentration dependence of high-frequency absorption in $La_{2-x}Sr_xCuO_4$ using ellipsometry. They found that a band at

2.0 eV, which is quite strong in undoped La_2CuO_4, becomes weaker at higher doping concentrations and is almost absent for $x > 0.10$. Similarly, Kelly *et al.*[72] and Garriga *et al.*[71] find that the spectrum of $YBa_2Cu_3O_6$ has two rather narrow absorption bands at 1.7 eV and 4.1 eV, which decrease in strength as oxygen is added, until they disappear at $\delta \approx 0.5$. The band at 4.1 eV is particularly narrow, being only 0.2 eV wide in a $\delta \approx 0.9$ sample. This band is interpreted as an excitation of $Cu^+(1)$ atoms of the tetragonal-phase, large δ material. The oscillator strength which is removed from these high-frequency features on doping presumably appears as dc and midinfrared oscillator strength.

Consistent with these studies is a photoconductivity study,[74] which determined the onset of direct transitions in $La_{2-x}Sr_xCuO_4$ to be at 2.6 eV, while the onset of direct transitions in La_2CuO_4 was at 2.2 eV. The observation of photoconductivity in conducting $La_{2-x}Sr_xCuO_4$ samples is interesting, suggesting that the carriers which participate in interband transitions have little interaction with the carriers responsible for the conductivity.

H. Photoinduced absorption

We end this section with a brief discussion of photoinduced absorption experiments.[75,76,77,78] In these studies, a sample of the nonsuperconducting, insulating phase, La_2CuO_4 or $YBa_2Cu_3O_{6.2}$ are illuminated with a high-frequency light source, typically a laser, and the absorption ratio between light on/light off is recorded. This ratio represents the excess absorption (or—if less than unity—the bleaching) due to the photoexcited carriers.

A photoinduced peak at 0.5 eV (4000 cm^{-1}) in La_2CuO_4 has been observed by two groups.[75,76] Additional features include photoinduced infrared vibrational modes[75] and at higher frequencies, photoinduced absorption at 1.4 eV and photoinduced bleaching at 2eV and above.[76] The former effect suggests strong electron-vibration coupling while the bleaching is consistent with a 2 eV gap in La_2CuO_4.

Similar effects are observed[77,78] in $YBa_2Cu_3O_{6.2}$. Here the photoinduced midinfrared band has a maximum at 0.12 eV (1000 cm^{-1}) but extends to quite high frequencies. Several phonon features are also seen in the photoinduced spectra. Thus the photoinduced spectra of the insulating phases of high T_c superconductors resemble in many ways the ordinary absorption spectra of the conducting phases.

IV. THE ENERGY GAP

A. Search for the gap in the ceramics

Guided by analogy to ordinary superconductors, which, at low temperature, have a region of essentially perfect reflectance at frequencies below the energy gap, much of the early infrared work on the new high temperature superconductors was aimed at finding the energy gap by reflectance techniques on pressed ceramic pellets. Within months of the announcement of the discovery of high T_c superconductivity a number of groups submitted reports on the low temperature far-infrared spectra.

In the normal state, the $La_{2-x}Sr_xCuO_4$ pellets showed the high far infrared reflectivity characteristic of free carriers, as expected from the metallic dc resistance behavior. In the superconducting state a prominent edge appeared in the 50 cm^{-1} region.[79–85] The position of the edge had a temperature dependence that was very suggestive of the BCS energy gap in the dirty limit. Fig. 17 shows the reflectance spectrum in $La_{2-x}Sr_xCuO_4$ ceramic as measured by Sherwin *et al.*[86] as a function of temperature. The edge at 60 cm^{-1} dominates the spectrum. If we were to identify it as superconducting gap, $2\Delta/k_BT_c \approx 1.6$–$2.5$, a very low value.

This interpretation of the 60 cm^{-1} edge as the onset of absorption at the energy gap of a dirty BCS superconductor leads to several problems. The first is the unexpectedly low energy of the gap found this way. The ratio $2\Delta/k_BT_c$ ranging from $\approx$ 1.6 to $\approx$ 2.5 is surprising since one had anticipated, in view of the very large transition temperature, a value suggestive of a strong coupling superconductivity, that is a value much larger than 3.5.

The second problem as shown by Bonn *et al.*[87] and by Sherwin *et al.*[86], is that a close examination of the optical constants of the effective medium of the

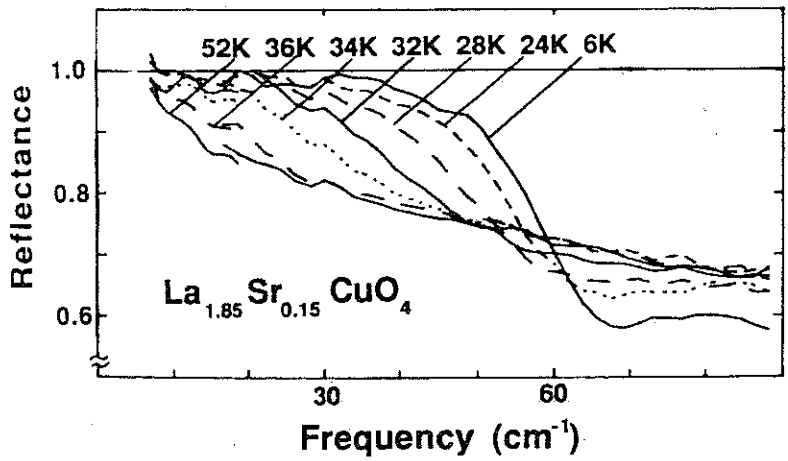

FIG. 17. Reflectance of a $La_{2-x}Sr_xCuO_4$ ceramic at various temperatures. The prominent temperature dependent edge has been interpreted as the superconducting energy gap and as a plasma edge. (After Sherwin *et al.*[86])

ceramic revealed that the edge at 60 cm^{-1} did not correspond to an onset of electronic absorption. Instead it arose from a zero-crossing of ϵ_1 of the composite material, with its mixture of grains with various orientations of the low conductivity c axis . Such a reflectance edge, when caused by a sign change in the real part of the dielectric function, is called a plasma edge in ordinary conductors, and it occurs at the screened plasma frequency. In a normal metal this frequency is rather high, occurring in the ultraviolet.

In the oxide ceramics the conduction electrons have a low density and their negative contribution to ϵ_1 at low frequency is relatively weak. A positive contribution from *any* absorption band can cause ϵ_1 to become positive at low frequency resulting in a premature zero crossing of this quantity. It is at such a zero crossing that the reflectivity develops a characteristic edge. In the case of the $La_{2-x}Sr_xCuO_4$ ceramics there are two sources of absorption that make a positive contribution to ϵ_1: the strong midinfrared band and a strong phonon absorption at 250 cm^{-1}, polarized in the c direction.[67]

Sherwin *et al.*[86] have analysed in detail the temperature dependence of such a plasma edge in a hypothetical BCS superconductor but with normal state optical constants appropriate to the $La_{2-x}Sr_xCuO_4$ ceramics. The position of the edge depends on an interplay between the positive contribution of the finite frequency oscillators and the negative contribution from the pure inductive response of the superconducting condensate at zero frequency. As the temperature

is increased from absolute zero the condensate fraction decreases and with it the negative contribution to ϵ_1. As a result the edge moves to lower frequencies and the position of the edge mimics the temperature dependence of the BCS energy gap.

This can be seen from the London model. From Eq. (21) in Section II, the superconductor has a dielectric function given by

$$\epsilon_1 = \epsilon_\infty - \frac{\omega_{ps}^2}{\omega^2}$$

where for this discussion, the first term, ϵ_∞ is dominated by the contribution from the oscillators, assumed to be constant at low frequency, and the second is the contribution from the superfluid condensate, i.e., the inertial response of the superconducting electrons. This expression is zero at

$$\omega = \sqrt{\frac{4\pi n_s e^2}{m^* \epsilon_\infty}}$$

where n_s is the density of superconducting electrons.

In the absence of strong absorption from the lattice or from interband effects, the reflectance will have a deep minimum at this frequency. Taking ϵ_∞ to be temperature independent, this expression can be used to determine the temperature dependence of n_s. Fig. 18 shows as a function of reduced temperature both the BCS gap and the reflectance edge based on this model. The temperature dependences of the two functions are very similar. There is some ambiguity in the density of the condensate determined by this simple argument since in the presence of damping it is not always easy to determine the zero crossing point of ϵ_1 from an examination of various features of the reflectance edge.

Sherwin *et al.*[86] conclude that it is not possible, on the basis of far infrared measurements of the reflectance edge, to determine whether the low frequency feature in the $La_{2-x}Sr_xCuO_4$ is the BCS energy gap or a plasma edge caused by the zero crossing of ϵ_1.

A similar edge appears in the $YBa_2Cu_3O_{7-\delta}$ ceramics at 220 cm^{-1} giving $2\Delta/k_BT_c \approx 3.5$ (there is another, sharper one associated with the 150 cm^{-1} phonon). A large number of investigators[29,88–98] have interpreted this as evi-

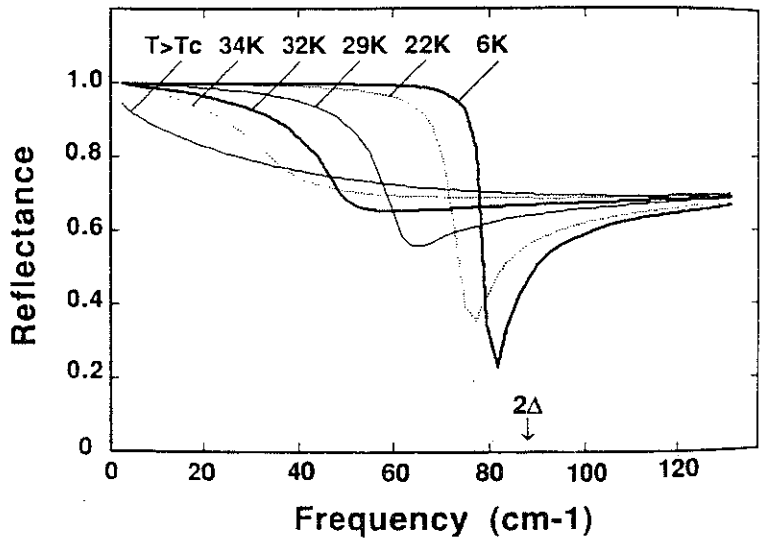

FIG. 18. Calculated reflectance at various temperatures from a model for a BCS superconductor that has a strong phonon in addition to the free carriers. The arrow denotes the position of the assumed superconducting gap. There is no obvious feature in the calculated reflectance spectrum at the gap frequency. (From Sherwin *et al.*[86]).

dence of a BCS energy gap at this frequency. The position of this edge depends on the method of sample preparation[56] but in ceramics with well annealed and undamaged surfaces the reflectance does drop rapidly in the region of 220 cm^{-1} as shown in Fig. 19.

Kramers-Kronig analysis[87,56,99] shows that this shoulder, observed in reflectance in $YBa_2Cu_3O_{7-\delta}$ceramics at low temperature, is not due to a well defined gap in the conductivity as expected for a BCS superconductor.[18] Instead it is partly caused by the strong dispersion contributed by the phonon pair at 277 cm^{-1} and 311 cm^{-1} that affect the effective-medium optical properties. The strong midinfrared absorption adds another important positive term to ϵ_1. The net effect is the pronounced reflectance decrease seen at 220 cm^{-1}. The underlying continuous electronic conductivity of the ceramic does not exhibit a gap in this region. The conductivity of this sample is shown in Fig. 20. The conductivity has no BCS-like gap at the frequency where the reflectance edge is observed. The sharp features seen in the reflectance spectrum transform to sharp phonon peaks superimposed on a smoothly rising continuous background; thus, they cannot be associated with the gap either.

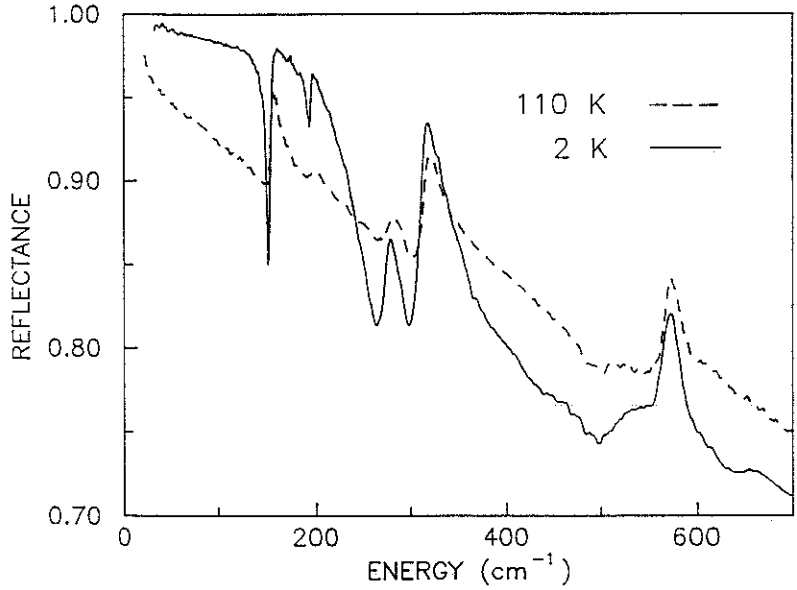

FIG. 19. Reflectance of a ceramic pellet of $YBa_2Cu_3O_{7-\delta}$ at two temperatures, one above the superconducting transition and the other well below it. The prominent edge at 220 cm^{-1} has been interpreted as a signature of the superconducting energy gap. Kramers Kronig analysis shows however that this feature is associated with the strong dispersion associated with the phonons and the midinfrared band.

Nevertheless it is important to note that the frequency dependent conductivity is reduced in the far infrared region in the superconducting state. The characteristic frequency range of this reduction is of the order of 3.5 kT_c in both $La_{2-x}Sr_xCuO_4$ and $YBa_2Cu_3O_{7-\delta}$.[82,56,99] Unlike a BCS superconductor where a region of true zero conductivity is observed,[100] the conductivity in the ceramics of the high temperature superconductors is not zero at far-infrared frequencies.

Although the phonon peaks confuse the reflectance spectrum, they also provide an indirect measurement of the energy gap. Phonon absorption features have finite widths caused by impurities, anharmonicity, and electron phonon interaction. In the superconducting state, phonons with frequency smaller than 2Δ lose the width caused by the electron phonon interaction because they do not have enough energy to break Cooper pairs. Hence phonons with $\omega < 2\Delta$ narrow upon entering the superconducing state. This has been observed[56] in $YBa_2Cu_3O_{7-\delta}$ where the phonons at 155 cm^{-1} and 195 cm^{-1} narrow upon cooling, but the phonons above 279 cm^{-1} do not. This suggests that the gap

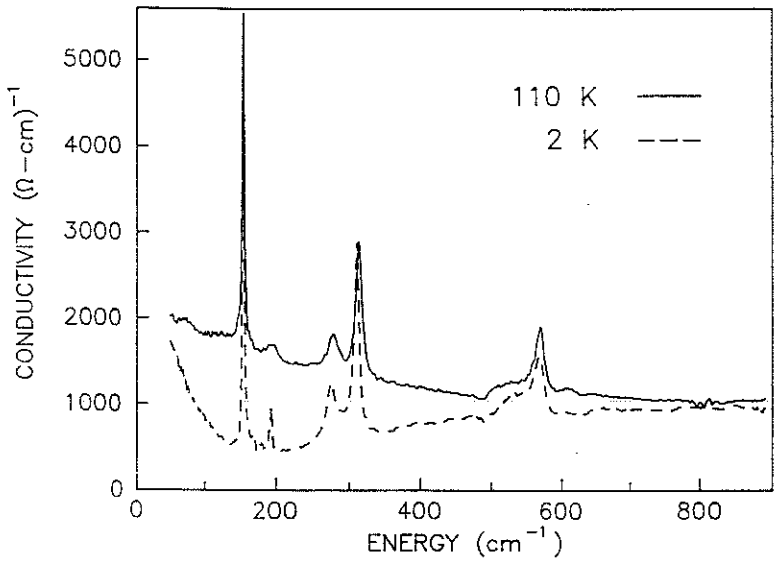

FIG. 20. The optical conductivity of a $YBa_2Cu_3O_{7-\delta}$ ceramic pellet. In the normal state at 110 K the conductivity is characterized by a rising free carrier part superimposed on a uniform background associated with the midinfrared band. Superimposed are several sharp phonon bands. On entering the superconducting state the free carrier conductivity is markedly reduced in the 100 to 300 cm^{-1} region but there is no evidence of a sharp gap. At the lowest frequencies the conductivity rises, as expected from the low-frequency behavior of the reflectance, shown in Fig. 19.

lies between 195 and 279 cm^{-1} ($3.0 < 2\Delta/k_BT_c < 4.3$).

In summary, the far infrared reflectance spectra of ceramic samples of the high temperature superconductors show shoulders that superficially resemble the energy gap of a BCS superconductor. However, these shoulders can be attributed to changes in the real part of the dielectric function associated with phonons and with the gradual onset of strong midinfrared absorption. Kramers-Kronig analysis gives a more detailed picture showing that while the far infrared conductivity is depressed in the superconducting state no true gap in the conductivity can be discerned.

The failure to observe a true energy gap by far-infrared spectroscopy in the ceramics can be traced to several causes. Firstly, non-superconducting material present on the surfaces of the specimens. Surface analysis techniques show small concentrations of minority phases in some samples, materials that originate from the crucible such as Al or Pt, as well as components of unreacted material such

as CuO.[59] Aluminum is known to suppress the transition temperature[101] and presumably, the energy gap.

Secondly there is the problem of **c** axis anisotropy. Measurements of dc electrical conductivity show that at low temperature the electron transport is very anisotropic: metallic if the currents flow in the **ab** plane and almost insulating in the **c** direction.

Finally the $YBa_2Cu_3O_{7-\delta}$ material is often heavily twinned with very small regions of alternating **a** and **b** direction domains. It is possible that the domain wall region is one with reduced oxygen content which could depress the gap locally.

B. The gap in ab-plane oriented crystals

To eliminate the uncertainties arising from anisotropy in polycrystalline, unoriented samples, single crystal studies are desirable. Radiation polarized along the various crystallographic direction can be used to obtain the corresponding optical conductivities. For simple reflectance spectroscopy in the energy gap region, 100 - 600 cm^{-1} , measurements on flat surfaces several millimeters in size, are needed. Crystals large enough to study both the two **ab**-plane directions and the **c** axis in the far infrared are not available at the time of writing of this review. The typical crystal that does exist is a very thin plate up to 3 by 3 mm in size in the **ab** plane and less than 0.1 mm thick in the **c** direction. In the **ab** plane there is considerable twinning: the largest untwinned regions are less than 100 μm in size.[102,65] It is for this reason that all the far-infrared measurements on crystals to date are unpolarized averages over the **a** and **b** directions of twinned specimens. No far-infrared spectra have been reported for light polarized in the **c** direction for superconducting samples.

The first absolute reflectance curves for $YBa_2Cu_3O_{7-\delta}$ in the long wavelength region where the energy gap is expected to appear are the measurements of Bonn *et al.*[57] on a mosaic of **ab** plane twinned crystals. Fig. 21 shows the reflectance at two temperatures, in the normal and superconducting states. There is no evidence of unit reflectance in the superconducting state that could be used to identify an energy gap. The reflectance is high at low frequency but there is residual absorption of the order of a few percent in the 200 – 500 cm^{-1}

region. The material was grown in an alumina crucible, and the unintentional Al doping suppresses T_c[101] somewhat, but this kind of residual absorption is also seen in most crystals grown in zirconia crucibles.[103] There is no sign of the characteristic signature of a BCS type of energy gap in this material: a region of unit reflectance followed by a rapid decrease to the normal state reflectance.

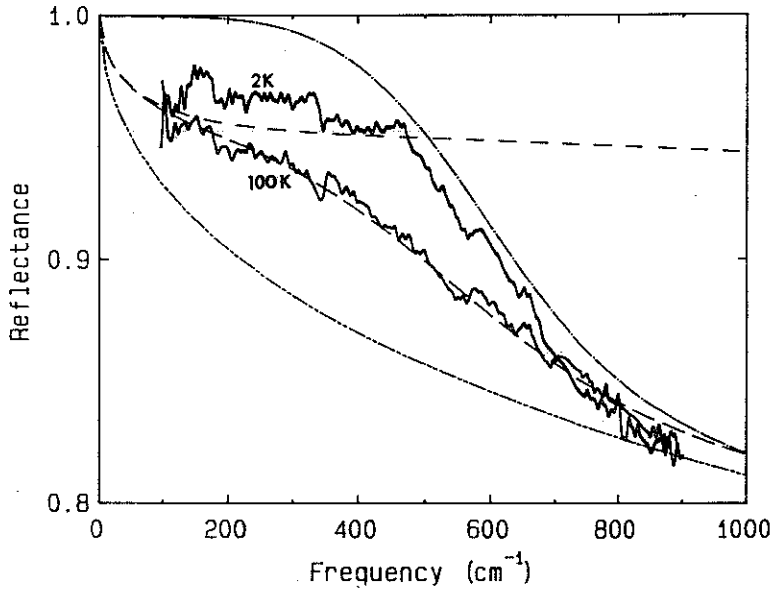

FIG 21. Reflectance of a mosaic of crystals oriented with the **ab** plane normal to the plane of incidence. The normal state reflectance is dominated by a region of negative curvature in the 400 cm^{-1} region, which becomes more prominent in the superconducting state. There is no evidence of a superconducting gap in this spectrum. The two dashed lines with positive curvature are fits to Drude models with different damping constants. The two curves with negative curvature include a midinfrared oscillator; the lower one is a least squares fit to the 100 K reflectance, the upper one uses the same parameters, but the Drude damping has been reduced to zero.

A detailed analysis of the optical properties of this sample[58,59] shows that in the normal state the conductivity can be described by a Drude term with a damping of 250 cm^{-1} at 100 K plus an oscillator to account for the midinfrared band. The onset of the midinfrared band is responsible for the region of negative curvature in the 500 cm^{-1} region. This hump is characteristic of many crystal samples of $YBa_2Cu_3O_{7-\delta}$.[103]

Calculations using the Mattis Bardeen formula show that any superconducting gap of the order of 200 cm^{-1} or larger does not produce an observable fea-

ture in the reflectance spectrum.[59] This is because already at 100 K the material is close to the clean limit, where $2\Delta > 1/\tau$. On account of the temperature dependence of the conductivity, one expects an even smaller damping rate at lower temperatures. In the dirty limit a strong shoulder develops in the reflectance at the gap frequency whereas in the clean limit there is no discernible feature at 2Δ. The physical reason for the disappearance of the gap in the case of very pure materials is the lack of collision processes that conserve momentum during the absorption of a photon. In contrast to the case of a semiconductor, where the gap is tied to the lattice potential, the superconducting gap is of electronic origin and cannot absorb the momentum of an excited electron[104].

Perhaps the strongest case for the observation of a superconducting gap by infrared techniques is the work of Thomas *et al.*[63] who report on the **ab**-plane properties of crystals of $YBa_2Cu_3O_{7-\delta}$ deliberately treated to yield a sample with reduced oxygen content and depressed transition temperature. Fig. 22 shows the absolute reflectance in the low frequency region of one of the samples. The authors argue that the region of high reflectance with the characteristic break at 150 cm^{-1} for the 68 K material represents the superconducting gap.

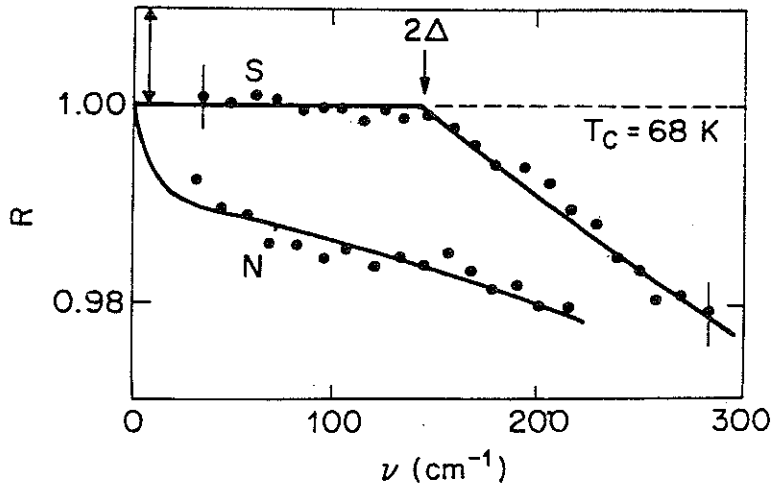

FIG. 22. Reflectivity of an oxygen depleted superconductor $YBa_2Cu_3O_{7-\delta}$. The authors interpret the region of unit reflectance below 150 cm^{-1} as the superconducting gap. (After Thomas *et al.*[63])

There are several conditions that must be met before a reflectance shoulder can legitimately be identified as a superconducting gap. First the absolute re-

flectance should be unity up to the gap. Within the quoted 2 % error limits, the curve of Thomas *et al.*[63] meets this condition . Secondly the feature should not be present in the normal state. There seems to be no region of positive curvature in the 100 – 200 cm^{-1} region that sharpens up to become the break at 150 cm^{-1} in the superconducting state. As a final check the material should not be in the clean limit. This last condition is difficult to test since we do not know what the Drude relaxation rate is in the superconducting state at low temperature. Thomas *et al.*[63] claim that in the normal state $1/\tau \sim 2k_BT$. At 100 K this gives a value of $1/\tau = 140$ cm^{-1}. If the normal-state resistivity levelled off below 100 K, so that the value $1/\tau = 140$ cm^{-1} persisted to low temperatures, then the sample would not be in the clean limit and the feature observed at 150 cm^{-1} by Thomas *et al.*[63] has a good chance of being the superconducting gap. A value of $2\Delta/k_BT_c \approx 3.5$ is obtained from this gap value and the 68 K transition temperature of the sample.

A much higher value of $2\Delta/k_BT_c$ is reported by Schlesinger *et al.*[38,105] Only reflectance ratios between the superconducting and normal states, R_s/R_n of a mosaic of aligned twinned crystals are given. The authors identify a shoulder that occurs at 480 cm^{-1} as the superconducting energy gap, so $2\Delta/k_BT_c \approx 7$ to 8. They do not observe unit reflectance at this frequency as one would expect for a bulk BCS superconductor. From their description it appears that the sample still has about 10 % absorption at 480 cm^{-1}. They suggest that presence of normal material causes this residual absorption.

The 480 cm^{-1} shoulder can be seen in the absolute reflectance curves of other investigators. Timusk *et al.*[58] associate it with the onset of the midinfrared absorption, whereas Thomas *et al.*[63] interpret it in terms of changes in the frequency dependent scattering rate.

Against the interpretation of shoulders such as the one at 480 cm^{-1} as superconducting gaps is an argument raised by Thomas *et al.*:[63] the reflectance does not rise to unity below this frequency as expected for a superconductor with a full BCS gap. Unit reflectance by itself does not guarantee that a shoulder is due to a superconducting gap. As we have seen in the discussion of the ceramics, the plasmon model of Sherwin *et al.*[86] yields a plateau of high reflectance with a gap-like shoulder, without the necessity of a gap. The same

mechanism appears to be operating at 480 cm^{-1}: the onset of the strong mid-infrared absorption pulls down the reflectivity and gives rise to an apparent shoulder.

The influence of the midinfrared absorption on reflectance in the 500 cm^{-1} region can be seen clearly in Fig. 23, from Thomas *et al.*[63] The reflectance shoulder that signals the onset of non-Drude behavior in the 400 – 500 cm^{-1} range can be seen at 200 K in the normal state and it seems to sharpen continuously until at 12 K, in the superconducting state, it becomes the sharp break at 480 cm^{-1}. In other words, if the 480 cm^{-1} feature is a gap, it is a gap that is already present in the normal state, only becoming sharper and better defined at low temperature.

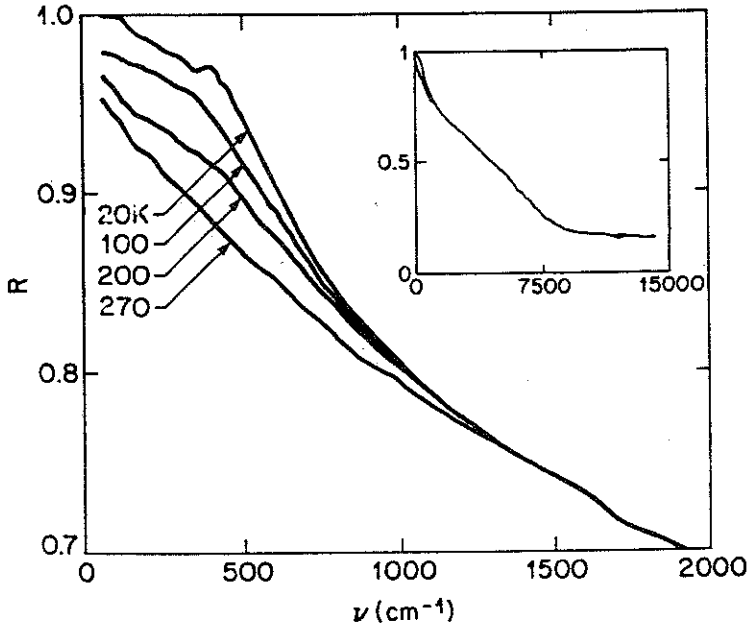

FIG. 23. Reflectivity of a crystal of $YBa_2Cu_3O_{7-\delta}$ with a transition temperature of 50 K. Note the characteristic region of positive curvature seen at low temperature in the 500 cm^{-1} region of the spectrum. It persists up to 200 K while at room temperature the spectrum takes on the characteristic Drude shape with a continuous positive curvature. (After Thomas *et al.*[63])

Recent work on $Bi_2Sr_2CaCu_2O_8$ by Reedyk *et al.*[106] gives further support to this view. Fig. 24 shows the reflectance of this material in the normal and superconducting states in the far infrared. In the normal state the conductivity

can be fit with a model that has two broad oscillators at 400 and 1000 cm^{-1} in addition to a Drude term centered at zero frequency.

In the superconducting state, within the experimental error of 0.5 %, the sample has unit reflectance below 300 cm^{-1}. This behavior is suggestive of a superconducting gap. However the oscillator needed to fit the normal state conductivity is close to this frequency, and quite possibly the sharp threshold is just a result of the sharpening of the low frequency edge of this oscillator, not the superconducting gap. Thus the 300 cm^{-1} shoulder in the $Bi_2Sr_2CaCu_2O_8$ has several of the necessary hallmarks of a superconducting gap, unit reflectance, a ratio R_S/R_n that superficially resembles the Mattis-Bardeen shape, and a marked sharpening in the superconducting state. Nevertheless it is very difficult to argue that this compound has a ***superconducting*** gap at this frequency since the structure is already present in the normal state.

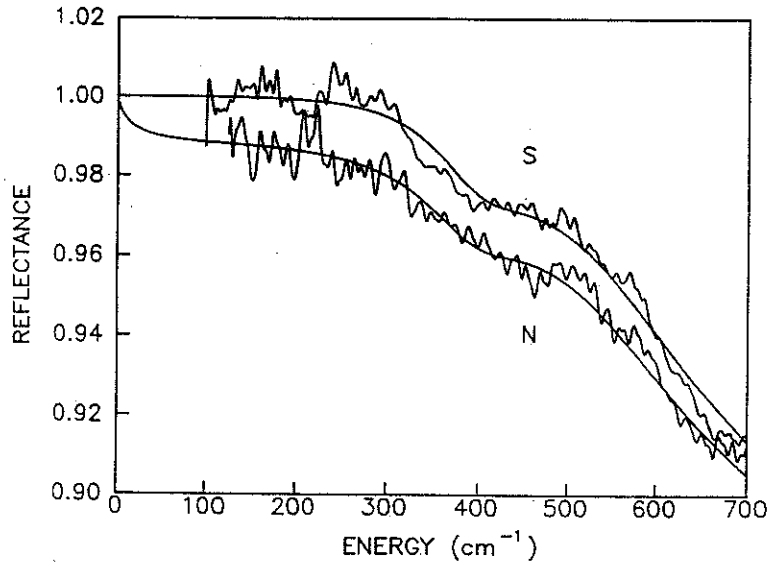

FIG. 24. Reflectance of $Bi_2Sr_2CaCu_2O_8$ in the far infrared. The normal state reflectance, marked N is very high at low frequency. The solid curve is a fit with with two oscillators at high frequency and a Drude term. The superconducting state, marked S, can be fit with the same oscillators but a Drude damping that is zero (solid smooth curve). In the 300 cm^{-1} region the experimental onset of absorption appears steeper than predicted by the model.

The difficulties of locating a superconducting gap in the crystals available at the time of writing this review are best illustrated in the recent work of the

AT&T group.[103] Reflectance curves for a large variety of crystal samples are given. There is a substantial amount of sample-to-sample variation but certain common features can be identified in the spectra:

(1) Good samples, defined as those having greater than 95 % absolute reflectance below 500 cm^{-1}, tend to show the 480 cm^{-1} shoulder in both the normal and the superconducting state.

(2) Poorer samples, those with lower reflectance, are more Drude-like: the reflectance curve has the uniform positive curvature expected for a Drude metal in the low frequency region. This is not too surprising: in the simple Drude picture, a high absorption at low frequency corresponds to a high scattering rate, which would tend to wash out any low-lying spectral features such as the shoulder at 480 cm^{-1}. In agreement the better samples tend to have a more washed out shoulder at higher temperature.

(3) The energy gap cannot be seen clearly in any of the samples. Having ruled out the 480 cm^{-1} shoulder as the gap, there is no evidence of a lower shoulder in any of the curves.

(4) There is some evidence for additional non-Drude behavior at the very lowest frequencies in the 50 to 100 cm^{-1} range in many of the samples. The reflectance seems to rise to unity at a finite, nonzero frequency. This could be consistent with a very low gap in the surface regions; it might be depressed by impurities or other defects.

At the time of writing of this review the gap question has not been settled: there is evidence in the work of Thomas *et al.*[63] for a rather low gap, of the order of 100 to 150 cm^{-1} magnitude in some oxygen deficient samples. These samples are characterized by very high normal state reflectances $R_n > 0.98$ at 200 cm^{-1} and perhaps have surface layers that are closer to the pure bulk superconductor than other samples. In other, perhaps less ideal, samples no gap can be identified in the 200 - 600 cm^{-1} region.

C. Other techniques

All the data presented so far was obtained by single-bounce reflectance, the most popular technique used in the study of the infrared properties of the

high temperature superconductors. In this section we will discuss other infrared techniques for finding the energy gap.

An alternative method of great potential sensitivity is the direct measurement of absorbed power by recording the temperature rise of a sample with a sensitive bolometer. The information provided by this technique is in principle not different from what is gained by reflectance, but the method is capable of great precision with small samples and with small absorption levels, as shown in studies of lead by Joyce and Richards[6] and in the organic conductor TTF-TCNQ by Eldridge and Bates[107]. The method has the disadvantage that the measurements have to be carried out in a narrow temperatures range matched to the region of sensitivity of the bolometer.

So far only ceramic samples have been measured. Gershenzon *et al.*[92] find in $YBa_2Cu_3O_{7-\delta}$ a threshold of absorption above 40 cm^{-1} that they identify with the energy gap. The material is not fully reflecting below this frequency but appears to have a residual absorption that can be estimated to be of the order of 1 % if we assume that the 200 cm^{-1} absorption is 30 %, typical of $YBa_2Cu_3O_{7-\delta}$ ceramics. Similarly Lee *et al.*[108] find that their sample of $YBa_2Cu_3O_{7-\delta}$ ceramic has an absorption on the order of 20 % below 200 cm^{-1}, rising strongly above this frequency. The characteristic phonon lines at 150 cm^{-1} and 195 cm^{-1} can be discerned.[108]

The bolometric method, when further refined, will be particularly useful with small crystals of very high reflectivity since the measurement of absolute reflectance to an accuracy better than 1 % is difficult by conventional single-bounce reflectance techniques.

Whereas bolometric measurements are made at constant temperature, microwave loss measurements are generally performed at constant frequency. In most cases the temperature dependence is studied. To extract an energy gap from surface impedance, a detailed theory is needed.[109] At low temperatures one can write the ratio of surface resistance in the superconducting state R_s to the normal state R_n as

$$\frac{R_s}{R_n} \sim e^{-\Delta/kT}.$$

This formula implies that the surface resistance would drop to zero at low temperature; in principle, one could find the energy gap from the tempera-

ture dependence. In practice, even conventional superconductors fail to follow this formula to the lowest temperature, always with some residual sample-dependent surface resistance. This residual absorption is much higher in the oxide superconductors.[110–113] Beyermann *et al.*[110] find, for example, a residual $R_s/R_n \approx 0.01$ at low temperature. They model this with a Lorentzian distribution of gap centered around $2\Delta/k_B T_c = 3.5$.

Porch *et al.*[113] studied $YBa_2Cu_3O_{7-\delta}$ powders diluted with Al_2O_3 at 5 GHz. Because of the difficulties with shape corrections, the absolute values of the conductivities σ_1 and σ_2 are subject to considerable error. Good results are obtained for the temperature dependence of σ_2. For example they find that σ_2, closely follows the clean limit BCS curve below T_c, (Fig. 25.) this behavior suggests that $2\Delta/k_B T_c$ is within 30% of the BCS weak coupling behavior. The real part of the conductivity σ_1 is more difficult to determine, especially as large additional losses above the expected BCS surface resistance were found. This behavior is consistent with other studies, both infrared and microwave.

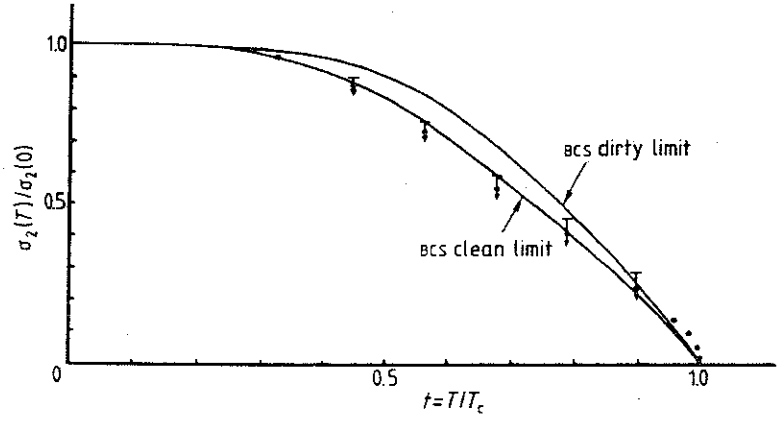

FIG. 25. The temperature dependence of the imaginary part of the conductivity (σ_2) of $YBa_2Cu_3O_{7-\delta}$ powders obtained by microwave measurements. The authors interpret these data with the clean limit BCS model, finding a gap within 30 % of the BCS value. (From Ref. 113.)

V. SUMMARY

A. The midinfrared absorption

Most recent infrared studies of the high T_c superconductors show that the far-infrared and the mid infrared properties are governed by different phenom-

ena, with the far-infrared conductivity being closely related to the dc transport properties whereas the midinfrared conductivity is dominated by some sort of low-lying excitation process. The crossover between the two regions occurs in the 0.05–0.13 eV (400–1000 cm^{-1}) region.

In discussing the midinfrared absorption, it is important to note that it occurs not only in the copper-oxide based superconductors, but also in many other systems. Barker,[114] in a study of the infrared properties of $SrTiO_3$ which had been made superconducting by reduction in hydrogen, observed that there was a strong midinfrared absorption in the superconducting materials. T_c in this material is low, but in other ways it resembles the copper-oxide materials. The broad infrared absorption, located at 0.25 eV (2000 cm^{-1}) has a peak conductivity of 100 $\Omega^{-1}cm^{-1}$, about a factor of ten smaller than in the high T_c superconductors.

A second material in which a midinfrared absorption occurs is the "old" high-T_c material, $BaPb_{1-x}Bi_xO_3$, which was studied in detail by Tajima *et al.*[115] It is important to note that unlike the new high T_c superconductors, $BaPb_{1-x}Bi_xO_3$ is a cubic material; hence, its dielectric function should be a scalar quantity. None of the issues of anisotropy or inhomogeniety arise in the discussion of this material.

$BaPb_{1-x}Bi_xO_3$ is a semiconductor for $x > 0.35$, a superconducting metal with $T_c \approx 10$ K for $0.20 \leq x \leq 0.35$, and a semimetal for small x. Samples in the superconducting range have a significant peak in the conductivity at approximately 0.5 eV (4000 cm^{-1}).[115] Fits to a model dielectric function similar to Eq. (23), including Drude, midinfrared, and ϵ_∞ terms, shows that the midinfrared absorption has about 75 % of the oscillator strength; the Drude 25 %. The midinfrared absorption is absent or much reduced in the low-T_c, $x \approx 0$ regime, although the σ_{dc} is still rather large. A final point of similarity is that when x is well into the semiconducting regime, the midinfrared band has been replaced by a 1.5–2 eV peak. In contrast to the copper-oxide high T_c superconductors, however, the location of the plasmon minimum in the reflectivity, which occurs near 1.5 eV (12,000 cm^{-1}) for $x \approx 0.27$, is strongly concentration dependent. Fits to Drude (or Drude plus Lorentzian) dielectric function models show that the square of the plasma frequency is a linear function of Bi concentration,

x. However, much of the increase at large x is clearly related to the growth and blue shift of the midinfrared absorption, and does not represent a linear increase in carrier concentration with x.

Finally, Kaplan *et al.*[116] have studied the infrared and optical properties of $La_4BaCu_5O_{13}$ and $La_2SrCu_2O_{6+\delta}$. As discussed by Torrance *et al.*[53] these materials have square-planar copper-oxide structures, are metallic (when $\delta > 0$), but are not superconducting. Kaplan *et al.* observed that $La_4BaCu_5O_{13}$ has a broad maximum at 1 eV (12,000 cm^{-1}) with a quasi-Drude, zero-frequency-centered peak dominant below 0.3 eV (3000 cm^{-1}). Unannealed samples of $La_2SrCu_2O_{6+\delta}$ (that is, samples with $\delta \approx 0$) have insulating behavior and no midinfrared absorption; those with increasing δ have a progressively stronger midinfrared absorption at 0.6 eV (5000 cm^{-1}). The center frequency of the infrared absorption is higher in these non-superconducting oxides than the 0.2–0.4 eV value found in $YBa_2Cu_3O_{7-\delta}$.

It seems that the common feature of the materials that display a strong midinfrared band is their mixed-valence nature. In La_2CuO_4, $YBa_2Cu_3O_6$, $SrTiO_3$, $BaBiO_3$, and $La_2SrCu_2O_6$ the valence of all ions is satisfied at their nominal values; in particular all of the oxygens are O^{2-}. When Sr or Pb are substituted for other ions or when oxygen is added or removed, the situation becomes complicated. The consensus at the present time seems to be that in the high T_c superconductors the holes reside on the planar oxygen atoms; if this is the case also in the other compounds, then the midinfrared absorption can be regarded as a signature of a significant concentration of O^- centers in the solid.

There are at least three ways of interpreting the midinfrared absorption:

(1) The effect is due to an emission of the excitation by the conduction carriers, i.e., a Holstein[7] process. In this indirect process, everything takes place in the conduction band and the *same* carriers are involved in both regimes, albeit with differing effective masses and lifetimes. This is the perspective taken by Thomas *et al.*[63] and Collins *et al.*[70]

(2) The midinfrared absorption is due to a direct excitation of some sort, which we call a "particle-hole" excitation. This excitation involves either a different set of carriers, a different initial state, or a different final state than the

dc transport. Herr *et al.*,[23] Kamarás *et al.*,[25] and, more recently, Timusk *et al.*[59] have taken this point of view.

(3) The absorption is due to a parallel channel of charge carriers with a very short, temperature independent relaxation time.

Two difficulties faced by the first interpretation were discussed in some detail in section IV. Briefly, the onset $\mathcal{E}$ of the Holstein processes should shift by 2Δ to higher frequencies when the material becomes superconducting; the midinfrared absorption, if anything, shifts to lower frequencies.[63,117] In addition, at temperatures where $k_B T \sim \mathcal{E}$ the dc resistivity should be strongly affected due to scattering of charge carriers by a thermal population of the excitations; the resistivity, however, remains linear over this temperature range.[45]

The interpretation in terms of a particle-hole excitation does not suffer from these problems. The superconducting gap would appear in the spectrum of the Drude carriers but would not necessarily affect the onset energies of particle-hole excitations. Similarly, if these excitations are weakly coupled to the conduction electrons, they would not affect the dc transport processes in any drastic way.

The third interpretation would lead to Drude response, governed at low frequencies by the long relaxation time but at high frequencies by the short relaxation time (remembering that for $\omega \gg 1/\tau$ the τ-dependence of the conductivity is $\sigma_1 \sim 1/\tau$). However, this notion is ruled out[59] by the lack of saturation of the dc resistance at high temperature. The high- frequency Drude parameters imply the temperature-independent part of the conductivity would be $\sigma_o \approx 1200$ $\Omega^{-1}\text{cm}^{-1}$. This is substantially larger than permitted by the measured high temperature conductivity,[45] which would give $\sigma_o \ll 300\ \Omega^{-1}\text{cm}^{-1}$.

There are several theories for the high T_c superconductors which give low-lying electronic transitions. It is beyond the scope of this review to give even an overview of the theory, but we mention here, in no particular order, a few papers which have addressed directly the optical properties.

Electronic band structure calculations can be used in principle to find the optical properties. This has been done for the $YBa_2Cu_3O_{7-\delta}$ system by Chui *et al.*[118] with quite interesting results. For $\delta \approx 0$ a strong midinfrared absorption is found, while for $\delta \approx 1$ this band is substantially reduced in intensity. This

result agrees qualitatively with the measurements of Kamarás *et al.*[25] on ceramic $YBa_2Cu_3O_{7-\delta}$ samples. Moreover, Chui *et al.* find that the midinfrared absorption, which is rather broad in unpolarized **ab**-plane spectra actually occurs at different frequencies for the two polarizations: 0.5 eV (4000 cm^{-1}) for $\mathbf{E} \parallel \mathbf{a}$ and 0.35 eV (2800 cm^{-1}) for $\mathbf{E} \parallel \mathbf{b}$. These values agree well with the results of Tanaka *et al.*[65]

The higher energy bands seem to be able to be well accounted for within ordinary electronic band structure pictures, with most calculations giving approximately 4–5 eV for the onset of many strong transitions and with the minimum direct interband gap being in the 1.7–2.2 eV range.[119,120]

The other approaches are generally based on the idea that the charge carriers suffer from strong Coulomb repulsion, making double occupancy of sites (especially Cu) unlikely. This approach leads to a correlated ground state, with low-lying electronic excitations of the charge transfer type, consisting of electrons being promoted from their ground-state orbital either to a neighboring site or to a different orbital on the same site. A wide variety of such transitions have been considered.

Shortly after the initial discovery of high T_c superconductors Varma, *et al.*[26] proposed that the superconductivity is mediated by charge transfer excitons from oxygen to copper. Taking an extended Hubbard picture, they proposed that the excitation consist of $Cu^{2+}O^{2-} \rightarrow Cu^{+}O^{-}$, etc., and predicted a band at $\approx$ 0.5 eV, governed by V, the near-neighbor term in the extended Hubbard model for two sites per unit cell.

A different charge-transfer picture has been presented by Weber[121] and by Jarrell *et al.*,[122] who consider charge transfer transitions between two d levels on Cu. They also find a band in the 0.4 eV region.

Interactions with the lattice have been considered by a number of workers. Here the picture is that a hole introduced by doping interacts strongly with the nearby Cu–O bonds, leading to the formation of a self-trapped polaron. The optical absorption associated with polarons has been discussed by Laughlin and Hanna[123] and by Rice and Wang.[124] Rice and Wang consider hole polarons, with the holes located mostly on the square-planar oxygen atoms surrounding

a particular Cu site. The lowest optical transition is then an excitation from a non-bonding O level to the half-filled Cu-O antibonding level. With the parameters chosen, this occurrs at 0.3–0.5 eV (2000–4000 cm^{-1}). In addition, they showed that electron-phonon coupling can lead to enhancements of the phonon absorption oscillator strength.

Magnetic ground states have been investigated widely, on account of the antiferromagnetic ground states of La_2CuO_4 and $YBa_2Cu_3O_6$. Schrieffer *et al.*[125] have constructed a "spin-bag" model by starting with a spin-density-wave (SDW) ground state for the insulating phases. This SDW state has a relatively large energy gap. On the introduction of holes through doping or increased oxygen content, the SDW gap is reduced. This reduction is not uniform; instead, it occurs only in the vicinity of the hole, forming a local distortion and trapping the hole in a manner analogous to a polaron. It is relatively straightforward to speculate about the optical absorption within this picture. The undoped state would be an insulator, and transitions across its SDW gap would be seen. Upon doping, a new absorption would appear at low frequencies, at an energy equal to the value of the gap within the bag. The oscillator strength of this absorption would grow with doping until the doping level becomes large enough to destroy the SDW order, when the strength should begin to decrease. Accompanying the initial increase in the low-energy band would be a corresponding decrease in the intensity of transitions across the original SDW gap. It is tempting to interpret the changes seen in $La_{2-x}Sr_xCuO_4$ upon doping[50], where a decrease in absorption in the 2.0 eV (16,000 cm^{-1}) range goes along with the increase in midinfrared absorption, in terms of this model, but no detailed calculations have as yet been carried out.

In summary, the midinfrared absorption in the high T_c superconductors, first seen in ceramic samples,[22,23,25] is also present in oriented **ab**-plane[56,59,63] samples. The nature of this absorption at the time of writing this review is undecided. We have discussed it in terms of a direct particle-hole excitation, but this still leaves many possibilities open. The working out of this fascinating puzzle, which itself is only part of the overall, multidimensional puzzle presented by the high T_c superconductors, will require further and better optical measurements, improved sample quality, and, no doubt, a number of new ideas.

B. The energy gap

At the time of the completion of this review there is little conclusive that can be said about the energy gap in the high T_c superconductors. Like the search for the Loch Ness monster, there have been many sightings but little tangible evidence. In this section we will briefly summarize our view of reasons for the lack of progress so far and suggest a possible route to the solution of the problem.

The main problem, from the beginning of the far infrared work on these fascinating materials, has been the complexity of the optical response. The copious structures produced by phonons in the polycrystalline materials and the strong midinfrared absorption in the **ab** plane oriented samples have hidden the subtle effects of the superconducting gap.

Even when these perturbations are taken into account, the gap is difficult to discern. The very pure materials approach the clean limit, and the threshold of conductivity that is predicted to appear at 2Δ by Mattis and Bardeen is very weak and overwhelmed by the inevitable noise. In the very dirty materials on the other hand, both T_c and the gap appear to be depressed. As a result, in the region of the expected gap ≈ 250 cm^{-1}, there is a residual absorption of a few percent, resulting possibly from surface regions where the average gap is well below this frequency.

From these considerations it appears that a compromise has to be struck. For the gap to be visible in the conductivity, the sample cannot be too pure and it cannot be too dirty. Of the data so far, the first polycrystalline ceramic samples of Bonn *et al.*[82,87] and the oxygen depleted samples of Thomas *et al.*[63] seem to fall into the middle ground, and show some evidence of a gap in the region expected for a BCS superconductor.

Other samples appear to be either in the clean limit (examples are the **ab** oriented ceramics of Bonn *et al.*[56] and of Ose *et al.*[99]) or else have contaminated surface layers where the gap, if it present at all, is depressed below the far infrared spectral region. This contamination is seen in most of the single crystal work to date.

It is puzzling that all the samples nevertheless show high T_c superconductivity according to four-probe resistance measurements. It appears that current-

carrying channels of undisturbed good superconductor exist between domains of low-gap material.

The problem of the observation of the gap is related to the very short coherence length, a few lattice spacings at most. To increase the scattering rate to the point where the dirty limit is approached, the mean free path has to become of the order of the coherence length, in this case only a few lattice spacings. In classic superconductors the defects that scatter the electrons have no effect on the gap and the true gap can be observed in the dirty limit. In high T_c superconductors, however, many defects have a very detrimental effect on T_c. Thus it appears that one cannot make the scattering length too short and still expect to see the intrinsic gap of the pure material.

Acknowledgements

"May you live in interesting times!" is supposed to be an ancient Chinese curse, but for those of us fortunate enough to have worked in the area of high T_c superconductors during the past two years, these have been interesting times indeed. The research from the McMaster-Florida collaboration that we have described here is the result of the skill and hard work of our students and postdoctoral associates: Doug Bonn, Mona Doss, Steve Herr, Kati Kamarás, Charles Porter, and Maureen Reedyk. John Greedan with Jim Garrett and Carl Stager have been an invaluable source of many well characterized high-quality samples. We are grateful to Siu-Wai Chan, Shahab Etemad, Laura Greene, and J.-M. Tarascon for their collaboration in this research. We have had stimulating discussions with G.L. Carr, J.A. Berlinsky, P. Hirshfeld, S. Jeyadev, C. Kallin, P. Kumar, A.J. Millis, J. Orenstein, M.J. Rice, J.R. Schrieffer, G.A. Thomas, C. Varma, and P. Wölfle.

Research at Florida was supported initially by the National Science Foundation—Solid State Chemistry—DMR-8416511 and is currently supported by DARPA grant MDA972-88-J-1006. At McMaster the support has come from the National Science and Engineering Research Council (NSERC) and The Canadian Institute for Advanced Research (CIAR).

REFERENCES

1. J.G. Bednorz and K.A. Müller, *Z. Phys. B* **64,** 189 (1986)
2. M.A. Biondi and M.P. Garfunkel, *Phys. Rev. Lett* **2,** 143, (1959); see also *Phys. Rev.* **116,** 853, (1959); *Phys. Rev.* **116,** 862, (1959).
3. R.E. Glover, III, and M. Tinkham, *Phys. Rev.* **108**, 243 (1957).
4. D.M. Ginsberg and M. Tinkham, *Phys. Rev.* **118**, 990 (1960).
5. P.L. Richards and M. Tinkham, *Phys. Rev.* **119**, 575 (1960).
6. R.R. Joyce and P.L. Richards, *Phys. Rev. Lett.* **24**, 1007 (1970).
7. T. Holstein, *Phys. Rev* **96**, 539, (1954); *Ann. Phys. (N.Y.)* **29**, 410, (1964).
8. P.B. Allen, *Phys. Rev. B* **3**, 305 (1971).
9. B. Farnworth and T. Timusk, *Phys. Rev. B* **14**, 5119 (1976).
10. Frederick Wooten, *Optical Properties of Solids* (Academic Press, New York, 1972).
11. Max Born and Emil Wolf, *Principles of Optics* (Pergamon Press, Oxford, 1980).
12. Miles V. Klein and Thomas E. Furtak, *Optics*, Second Ed. (Wiley, New York, 1986).
13. Charles Kittel, *Introduction to Solid State Physics*, Fifth Ed. (Wiley, New York, 1976).
14. H. Mori, *Prog. Theor. Phys.* **34,** 399, (1965).
15. W. Götze and P. Wölfle, *Phys. Rev. B* **6**, 1226 (1972).
16. J.W. Allen and J.C. Mikkelsen, *Phys. Rev. B* **15**, 2952 (1977).
17. D. Penn, *Phys. Rev.* **128**, 2093 (1962).
18. D.C. Mattis and J. Bardeen, *Phys. Rev.* **111**, 412 (1958).
19. L. Leplae, Ph.D. Thesis, University of Maryland, (1962); *Phys. Rev. B* **27**, 1911 (1983).
20. D.M. Ginsberg, *Phys. Rev.* **151,** 241, (1966), D.R. Karecki, G.L. Carr, S. Perkowitz, D.U. Gubser, and S.A. Wolf, *Phys. Rev. B* **27**, 5460 (1983).
21. S. Tajima, S. Uchida, S. Tanaka, S. Kanbe, K. Kitazawa, and K. Fueki, *Jpn. J. Appl. Phys.* **26**, L432 (1987).
22. J. Orenstein, G.A. Thomas, D.H. Rapkine, C.B. Bethea, B.F. Levine, R.J. Cava, E.A. Reitman, and D.W. Johnson, Jr., *Phys. Rev. B* **36**, 729 (1987).
23. S.L. Herr, K. Kamarás, C.D. Porter, M.G. Doss, D.B. Tanner, D.A. Bonn, J.E. Greedan, C.V. Stager, and T. Timusk, *Phys. Rev. B* **36**, 733 (1987).

24. D.A. Bonn, J.E. Greedan, C.V. Stager, T. Timusk, M.G. Doss, S.L. Herr, K. Kamarás, and D.B. Tanner, *Phys. Rev. Lett.* **58**, 2249 (1987).

25. K. Kamarás, C.D. Porter, M.G. Doss, S.L. Herr, D.B. Tanner, D.A. Bonn, J.E. Greedan, A.H. O'Reilly, C.V. Stager, and T. Timusk, *Phys. Rev. Lett.* **59**, 919 (1987).

26. C.M. Varma, S. Schmitt-Rink, and E. Abrahams *Solid State Comm.* **62**, 681 (1987).

27. J. Orenstein and D.H. Rapkine, *Phys. Rev. Lett.* **60**, 968 (1988).

28. Z. Schlesinger, R.T. Collins, M.W. Schafer, and E.M. Engler, *Phys. Rev. B* **36**, 5275 (1987).

29. G.A. Thomas, A.J. Millis, R.N. Bhatt, R.J. Cava, and E.A. Rietman, *Phys. Rev. B* **36**, 736 (1987).

30. P.E. Sulewski, T.W. Noh, J.T. McWhirter, and A.J. Sievers, *Phys. Rev. B* **36**, 5735 (1987).

31. T.W. Noh, P.E. Sulewski, and A.J. Sievers, *Phys. Rev. B* **36**, 8866 (1987).

32. G.L. Doll, J. Steinbeck, G. Dresselhaus, M.S. Dresselhaus, A.J. Strauss, H.J. Steiger, *Phys. Rev. B* **36**, 8884 (1987).

33. X. Wang, T. Nanba, M. Ikezawa, Y. Isikawa, K. Mori, K. Kobayashi, K. Kasai, K. Sato, and T. Fukase, *Jpn. J. Appl. Phys.* **26**, L1391 (1987).

34. G.L. Doll, J.T. Nicholls, M.S. Dresselhaus, A.M. Rao, J.M. Zhang, G.W. Lehmann, P.C. Eklund, G. Dresselhaus, and A.J. Strauss, *Phys. Rev. B* submitted.

35. T. Koide, H. Fukutani, A. Fujimori, R. Suzuki, T. Shidara, T. Takahshi, S. Hosoya, and M. Sato, *Jpn. J. Appl. Phys.* **26-3**, 915 (1987).

36. S. Tajima, S. Uchida, H. Ishii, H. Takagi, S. Tanaka, U. Kawabe, H. Hasegawa, T. Aita, and T. Ishiba, *Mod. Phys. Lett. B* **1**, 353 (1988).

37. P.E. Sulewski, T.W. Noh, J.T. McWhirter, A.J. Sievers, S.E. Russek, R.A. Buhrman, C.S. Jee, J.E. Crow, R.E. Salomon, amd G. Myer, *Phys. Rev. B* **36**, 2357 (1987).

38. Z. Schlesinger, R.T. Collins, D.L. Kaiser, and F. Holtzberg, *Phys. Rev. Lett.* **59**, 1958 (1987).

39. J. Orenstein, G.A. Thomas, D.H. Rapkine, C.B. Bethea, B.F. Levine, B. Batlogg, R.J. Cava, D.W. Johnson, Jr., and E.A. Rietman, *Phys. Rev. B* **36**, 8892 (1987).

40. I. Bozovic, K. Char, S.J.B. Yoo, A Kapitulnik, M.R. Beasley, T.H. Geballe, Z.Z. Wang, S. Hagen, N.P. Ong, D.E. Aspnes, and M.K. Kelly, *Phys. Rev. B* **38**, 5077 (1988).

41. R.T. Collins, Z. Schlesinger, R.H. Koch, R.B. Laibowitz, T.S. Plaskett, P. Freitas, W.J. Gallagher, R.L. Sandstrom, and T.R. Dinger, *Phys. Rev. Lett.* **59**, 704 (1987).

42. I. Bozovic, D. Kirillov, A. Kapitulnik, K. Char, M.R. Hahn, M.R. Beasley, T.H. Geballe, Y.H. Kim, and A.J. Heeger, *Phys. Rev. Lett.* **59**, 2219 (1987).

43. K. Kamarás, C.D. Porter, M.G. Doss, S.L. Herr, D.B. Tanner, D.A. Bonn, J.E. Greedan, A.H. O'Reilly, C.V. Stager, and T. Timusk, *Phys. Rev. Lett.* **60**, 969 (1988).

44. J.M. Tarascon, W.R. McKinnon, L.H. Greene, G.W. Hull, and E.M. Vogel, *Phys. Rev. B* **36**, 226 (1987).

45. M. Gurvitch and A.T. Fiory, *Phys. Rev. Lett.* **59**, 1337 (1987).

46. D.A. Bonn, J.E. Greedan, C.V. Stager, T. Timusk, K. Kamarás, C.D. Porter, M.G. Doss, S.L. Herr, and D.B. Tanner, *Rev. Solid State Sci.* **1**, 349 (1987).

47. D.R. Harshman, G. Aeppli, E.J. Ansoldo, B. Batlogg, J.H. Brewer, J.F. Carolan, R.J. Cava, M. Celio, A.C.D. Chaklader, W.N. Hardy, S.R. Kreitzman, G.M. Luke, D.R. Noakes, and M. Sheba, *Phys. Rev. B* **36**, 2368 (1987).

48. Y.J. Uemura, V.J. Emery, A.R. Moodenbaugh, M. Suenaga, D.C. Johnston, A.J. Jacobsen, J.T. Lewandowski, J.H. Brewer, R.F. Kiefl, S.R. Kreitzman, G.M. Luke, T. Riseman, C.E. Stronach, W.J. Kossler, J.R. Kempton, X.H. Yu, D.Opie, and H.E. Schone, *Phys. Rev. B* **38**, 909 (1988).

49. A.T. Fiory, A.F. Hebard, P.M. Mankiewich, and R.E. Howard, *Phys. Rev. Lett.* **61**, 1419 (1988).

50. S. Etemad, D.E. Aspnes, M.K. Kelly, R. Thomson, J.-M. Tarascon, and G.W. Hull, *Phys. Rev. B* **37**, 3396 (1988).

51. S. Etemad, D.E. Aspnes, P. Barboux, G.W. Hull, M.K. Kelly, J.M. Tarascon, R. Thompson, S.L. Herr, K. Kamarás, C.D. Porter, and D.B. Tanner, *Mat. Res. Soc. Symp. Proc.* **99**, 135 (1988).

52. S.L. Herr et al. in *High Temperature Superconducting Materials: Preparations, Properties and Processing,* edited by William Hatfield and J.J. Miller (Marcel Dekker, Inc., New York, 1988), p. 275.

53. J.B. Torrance, Y. Tokura, A.I. Nazzal, A. Bezinge, T.C. Huang, and S.S. Parkin, *Phys. Rev. Lett.* **61**, 1127 (1988).

54. K. Kamarás, M.G. Doss, S.L. Herr, J.S. Kim, C.D. Porter, G.R. Stewart, D.B. Tanner, D.A. Bonn, J.E. Greedan, A.H. O'Reilly, C.V. Stager, T. Timusk, B. Keszei, S. Pekker, Gy. Hutiray, and L. Mihály, *Mat. Res. Soc. Symp. Proc* **99**, 777 (1988).

55. J.M. Tarascon, L.H. Greene, W.R. McKinnon, G.W. Hull, and T.H. Geballe, *Science* **235**, 1373 (1987).

56. D.A. Bonn, A.H. O'Reilly, J.E. Greedan, C.V. Stager, T. Timusk, K. Kamarás, and D.B. Tanner, *Phys. Rev. B* **37**, 1547 (1988).

57. D.A. Bonn, A.H. O'Reilly, J.E. Greedan, C.V. Stager, T. Timusk, K. Kamarás, and D.B. Tanner, *Mat. Res. Soc. Symp. Proc.* **99**, 227, (1988).

58. T. Timusk, D.A. Bonn, J.E. Greedan, C.V. Stager, J.D. Garrett, A.H. O'Reilly, M. Reedyk, K. Kamarás, C.D. Porter, S.L. Herr, and D.B. Tanner, *Physica C* **153–155**, 1744 (1988).

59. T. Timusk, S.L. Herr, K. Kamarás, C.D. Porter, D.B. Tanner, D.A. Bonn, J.D. Garrett, C.V. Stager, J.E. Greedan, and M. Reedyk, *Phys. Rev. B* **38**, 6683 (1988).

60. D.B. Tanner, S.L. Herr, K. Kamarás, C.D. Porter, T. Timusk, D.A. Bonn, J.D. Garrett, J.E. Greedan, C.V. Stager, M. Reedyk, S. Etemad, and S.-W. Chan, *Synth. Met.* in press.

61. D.B. Tanner, T. Timusk, S.L. Herr, K. Kamarás, C.D. Porter, D.A. Bonn, J.D. Garrett, C.V. Stager, J.E. Greedan, and M. Reedyk, *Physica A* in press.

62. J. Orenstein, G.A. Thomas, D.H. Rapkine, A.J. Millis, L.F. Schneemeyer, and J.V. Waszczak, *Physica C* **153–155**, 1740 (1988).

63. G.A. Thomas, J. Orenstein, D.H. Rapkine, M. Capizzi, A.J. Millis, R.N. Bhatt, L.F. Schneemeyer, and J.V. Waszczak, *Phys. Rev. Lett.* **61**, 1313 (1988).

64. D. van der Marel, J. van Elp, G.A. Sawatzky, and D. Heitmann, *Phys. Rev. B* **37**, 5136 (1988).

65. J. Tanaka, K. Kamya, M. Shimizu, M. Simada, C. Tanaka, H. Ozeki, K. Adachi, K. Iwahashi, F. Sato, A. Sawada, S. Iwata, H. Sakuma, and S Uchiyama, *Physica C* **153–155**, 1752 (1988).

66. J. Tanaka, K. Kamiya, and S. Tsurumi, *Physica C* **153–155**, 653 (1988).

67. F. Gervais, P. Echegut, J.M. Bassat, and P. Odier, *Phys. Rev. B* **37**, 9364 (1988).

68. J. Tanaka, M. Shimada, U. Mizutani, and M. Hasegawa, *Physica C* **153–155**, 651 (1988).

69. J. Bassat, P. Odier, and F. Gervais, *Phys. Rev. B* **35**, 7126 (1987).

70. R.T. Collins, Z. Schlesinger, F. Holtzberg, P. Chaudhari, and C. Feild, preprint.

71. M. Garriga, U. Venkateswaren, K. Syassen, J. Humlicek, M. Cardona, Hj. Mattausch, and E. Schönherr, *Physica C* **153–155**, 643 (1988).

72. M.K. Kelly, P. Barboux, J.-M. Tarascon, D.E. Aspnes, W.A. Bonner, and P.A. Morris, *Phys. Rev. B* **38**, 870 (1988).

73. H.P. Geserich, B. Koch, G. Scheiber, J. Geerk, H.C. Li, G. Linker, W. Weber, and W. Assmus, *Physica C* **153–155**, 661 (1988).

74. F.A. Benko, G. Abdussalam, F.S. Razavi, and F.P. Koffyberg, *Phys. Rev. B* **38**, 2820 (1988).

75. Y.H. Kim, A.J. Heeger, L. Acedo, G. Stuckey, and F. Wudl, *Phys. Rev. B* **36**, 7252 (1987).

76. J.M. Ginder, M.G. Roe, Y. Song, R.P. McCall, J.R. Gaines, E. Ehrenfreund, and A.J. Epstein, *Phys. Rev. B* **37**, 7506 (1988).

77. Y.H. Kim, C.M. Foster, A.J. Heeger, S. Cox, and G. Stucky, *Phys. Rev. B* **38**, 6478 (1988).

78. C. Taliani, R. Zamboni, G. Ruani, F.C Matacotta, and K.I. Pokhodnya, *Solid State Comm.* **66**, in press (1988).

79. P.E. Sulewski, A.J. Sievers, S.E. Russek, H.D. Hallen, D.K. Lathrop, and R.A. Buhrman, *Phys. Rev. B* **35**, 5330 (1987).

80. U. Walter, M.S. Sherwin, A. Stacy, P.L. Richards, and A. Zettl, *Phys. Rev. B* **35**, 5327 (1987).

81. Z. Schlesinger, R.L. Greene, J.G. Bednorz, and K.A. Müller, *Phys. Rev. B* **35**, 5334 (1987).

82. D.A. Bonn, J.E. Greedan, C.V. Stager, and T. Timusk, *Solid State Comm.* **62**, 838 (1987).

83. G.A. Thomas, M. Capizzi, J. Orenstein, D.H. Rapkine, L.F. Schneemeyer, J.V. Waszczak, A.J. Millis, and R.N. Bhatt, *Jpn. J. Appl. Phys.* **26-3**, 1001 (1987).

84. Z. Schlesinger, R.T. Collins, and M.W. Schafer, *Phys. Rev. B* **35**, 7232 (1987).

85. L. Degiorgi, E. Kaldis, and P. Wachter, *Solid State Comm.* **64**, 873 (1987).

86. M.S. Sherwin, P.L. Richards, and A. Zettl, *Phys. Rev. B* **37**, 1587 (1988).

87. D.A. Bonn, J.E. Greedan, C.V. Stager, T. Timusk, M.G. Doss, S.L. Herr, K. Kamarás, C.D. Porter, D.B. Tanner, J.M. Tarascon, W.R. McKinnon, and L.H. Greene, *Phys. Rev. B* **35**, 8843 (1987).

88. T.H.H. Vuong, D.C. Tsui, V.J. Goldman, P.H. Hor, R.L. Meng, and C.W. Chu, *Solid State Comm.* **63**, 525 (1987).

89. L. Genzel, A. Wittlin, J. Kuhl, Hj. Mattausch, W. Bauhofer, and A. Simon, *Solid State Comm.* , 63, 843 (1987).

90. J.M. Wrobel, S. Wang, S. Gygax, B.P. Clayman, and L.K. Peterson, *Phys. Rev. B* **36**, 2368 (1987).

91. A.V. Bazhenov, A.V. Gorbunov, N.V. Klassen, S.F. Kondakov, I.V. Kukuskin, V.D. Kulakovskii, O.V. Misochlo, V.B. Timofeev, L.I. Chernyshova, and B.N. Shepel', *Jpn. J. Appl. Phys.* **26-3**, 893 (1987).

92. E.M. Gershenzon, G.N. Gol'tsman, B.S. Karasik, and A.D. Semenov, *Pis'ma Zh. Eksp. Teor. Fiz.*, **46**, 122 (1987); *JETP Lett.*, *48*, 151 (1987).

93. S. Perkowitz, G.L. Carr, B. Lou, S.S. Yom, R. Sudharsanan, and D.S. Ginley, *Solid State Comm.* **64**, 721 (1987).

94. M. Cardona, L. Genzel, R. Liu, A. Wittlin, Hj. Mattausch, F. García-Alvarado, and E. García-González, *Solid State Comm.* **64**, 727 (1987).

95. Y. Saito, H. Sawada, T. Iwazumi, Y. Abe, H. Ikeda, and R. Yoshizaki, *Solid State Comm.* **64**, 1047 (1987).

96. H. Ye, W. Lu, Z. Lu, X. Shen, B. Miao, Y. Cai, and Y. Qian, *Phys. Rev. B* **36**, 8802 (1987).

97. A. Wittlin, L. Genzel, M. Cardona, M. Bauer, W. König, E. Garcia, M. Barahona, and M.V. Cabañias, *Phys. Rev. B* **37**, 652 (1988).

98. P.J.M van Bentum, L.E.C. van de Leemput, L.W.M. Schreurs, P.A.A. Teunissen, and H. van Kempen, *Phys. Rev. B* **36**, 843 (1987).

99. W. Ose, P.E. Obermayer, H.H. Otto, T. Zetterer, H. Lengfellner, N. Tasler, J. Keller, and K.F. Renk, *Physica C* **153–155**, 639 (1988).

100. S.L. Norman and D.H. Douglass, *Phys. Rev. Lett.* **10**, 339 (1967).

101. J.P. Franck, J. Jung, and M.A.-K. Mohamed, *Phys. Rev. B* **36**, 2308 (1987).

102. N.P. Ong, Z.Z. Wang, S. Hagen, T.W. Jing, J. Clayhold, and J. Horvath, *Physica C* **153–155**, 1072 (1988).

103. G.A. Thomas, M. Capizzi, T. Timusk, S.L. Cooper, J. Orenstein, D. Rapkine, S. Martin, L.F. Schneemeyer, and J.V. Waszczak, *J. Opt. Soc. Am., Special Issue on Superconductivity* (submitted) 1989.

104. J. Hopfield, *Phys. Rev.* **139**, A419 (1964).

105. Z. Schlesinger, R.T. Collins, D.L. Kaiser, and F. Holtzberg, G.V. Chandrashekhar, M.W. Scafer, and T.M. Plaskett, *Physica C* **153–155**, 1734 (1988).

106. M. Reedyk, D.A. Bonn, J.D. Garrett, J.E. Greedan, C.V. Stager, T. Timusk, K. Kamarás, and D.B. Tanner, *Phys. Rev. B* in press.

107. J.E. Eldridge and F.E. Bates, *Phys. Rev. B* **28**, 6972 (1983).

108. M.W. Lee, T. Pham, H.D. Drew, S.M Bhagat, R.E. Glover III, S.H. Mosley, K.P. Stewart, and C. Lisse, *Solid State Comm.* **65**, 1135 (1988).

109. J.R. Waldram, *Advances in Physics* **13**, 1, (1964).

110. W.P. Beyermann, B.Alavi, and G. Grüner, *Phys. Rev. B* **35**, 8826 (1987).

111. S. Sridhar, C.A. Shiffman, and H. Hamdeh, *Phys. Rev. B* **36**, 2301 (1987).

112. M. Poirier, G. Quiron, K.R. Poppelmeier,and J.P. Thiel, *Phys. Rev. B* **36**, 3906 (1987).

113. A. Porch, J.R. Waldram, and L. Cohen, *J. Phys. F: Met. Phys.* **18**, 1547, (1988)

114. A.S. Barker, in *Optical Properties and Electronic Structure of Metals and Alloys,* edited by F. Abelés (North Holland, Amsterdam, 1965)

115. S.Tajima, S. Uchida, A. Masaki, H. Tagaki, K. Kitazawa, and S. Tanaka, *Phys. Rev. B* **32**, 6302 (1985).

116. S.G. Kaplan, T.W. Noh, P.E. Sulewski, H. Xia, A.J. Sievers, J. Wang, and R. Raj, *Phys. Rev. B* **38**, 5006 (1988).

117. C.D. Porter, S.L. Herr, K. Kamarás, D.B. Tanner, D.A. Bonn, J.E. Greedan, A.H. O'Reilly, and T. Timusk, unpublished.

118. S.T. Chui, R.V. Kasowski, and W.Y. Hsu, *Phys. Rev. Lett.* **61**, 885 (1988).

119. L.F. Mattheiss, *Phys. Rev. Lett.* **58**, 1028 (1987).

120. S. Massida, J. Yu, A.J. Freeman, and D.D. Koelling, *Phys. Lett.* **A122**, 198 (1987).

121. Werner Weber, *Z. Phys. B* **70**, 323 (1987).

122. Mark Jarrell, H.R. Krishnamurthy, and D.L. Cox, *Phys. Rev. B* **38**, 4584 (1988).

123. R.B. Laughlin, C.B. Hanna, in *Novel Superconductivity*, edited by S.A. Wolf and V. Z. Kreskin (Plenum, New York, 1987).

124. M.J. Rice and Y.R. Wang, *Phys. Rev. B* **36**, 8794 (1987).

125. J.R. Schrieffer, X.G. Wen, and S.C. Zhang, *Phys. Rev. Lett.* **60**, 944 (1988).